

Collider Tests of the Renormalizable Coloron Model

Yang Bai^{*} and Bogdan A. Dobrescu[◇]

^{*}*Department of Physics, University of Wisconsin-Madison, Madison, WI 53706, USA*

[◇]*Theoretical Physics Department, Fermilab, Batavia, IL 60510, USA*

February 8, 2018

Abstract

The coloron, a massive version of the gluon present in gauge extensions of QCD, has been searched for at the LHC as a dijet or top quark pair resonance. We point out that in the Renormalizable Coloron Model (ReCoM) with a minimal field content to break the gauge symmetry, a color-octet scalar and a singlet scalar are naturally lighter than the coloron because they are pseudo Nambu-Goldstone bosons. Consequently, the coloron may predominantly decay into scalar pairs, leading to novel signatures at the LHC. When the color-octet scalar is lighter than the singlet, or when the singlet mass is above roughly 1 TeV, the signatures consist of multi-jet resonances of multiplicity up to 12, including topologies with multi-prong jet substructure, slightly displaced vertices, and sometimes a top quark pair. When the singlet is the lightest ReCoM boson and lighter than about 1 TeV, its main decays (W^+W^- , γZ , ZZ) arise at three loops. The LHC signatures then involve two or four boosted electroweak bosons, often originating from highly displaced vertices, plus one or two pairs of prompt jets or top quarks.

Contents

1	Introduction	1
2	Renormalizable $SU(3)_1 \times SU(3)_2$ model	3
2.1	Bosonic mass spectrum	3
2.2	Interactions of the new bosons	5
2.3	Partial widths of the color-octet bosons	6
2.4	Partial widths of the singlet scalar ϕ_I	9
3	Production of scalars at the LHC	13
4	Novel LHC signatures	17
4.1	Light color-octet scalar: $M_{G'} > M_{\phi_I} > M_{\Theta}$	17
4.2	Light singlet scalar: $M_{G'} > M_{\Theta} > M_{\phi_I}$	20
4.2.1	$\phi_I \rightarrow ggq\bar{q}$	20
4.2.2	$\phi_I \rightarrow W^+W^-, \gamma Z, ZZ$	25
5	Discussion and conclusions	27
	Appendix: Ratios of scalar masses	31

1 Introduction

Massive elementary particles of spin-1 are well-behaved at high-energies only if they are associated with a spontaneously broken gauge symmetry [1]. The sector responsible for breaking the gauge symmetry necessarily includes additional bosons (Higgs-like scalars or composite ρ -like fields) that couple to the gauge boson, and are not much heavier (but could be much lighter) than it. As a result, the additional bosons may drastically affect the phenomenology of a new massive gauge boson (see, *e.g.*, [2, 3]).

The coloron [4–7] is a color-octet spin-1 particle that is present in gauge extensions of the QCD. The classic example [8–10] is an $SU(3)_1 \times SU(3)_2$ gauge symmetry broken down to the $SU(3)_c$ gauge group of QCD. If all SM quarks are triplets under one of the $SU(3)$ groups, then the coloron has flavor-universal couplings [6, 7], and dijet or top quark pair resonance searches at the LHC are sensitive to s -channel production of the coloron.

The spontaneous breaking of $SU(3)_1 \times SU(3)_2$ is usually assumed to be due to a bi-fundamental scalar field that acquires a diagonal vacuum expectation value (VEV).

A scalar potential that achieves that was considered in [6, 7], and involved a mass term and two quartic terms. It was pointed out in [2] that an additional term, of dimension 3, in the potential is consistent with the gauge and Lorentz symmetries. The presence of that dimension-3 term is in fact useful, as it leads to a mass for a Nambu-Goldstone boson that would otherwise be phenomenologically problematic. The regions of parameter space where the desired symmetry breaking pattern is achieved have been derived in [11]. We refer to the flavor-universal $SU(3)_1 \times SU(3)_2$ theory, with the most general terms of dimension up to four in the potential, as the Renormalizable Coloron Model (ReCoM).

Even though the ReCoM is a simple extension of the Standard Model (SM), its phenomenology is rich and has not been fully explored thus far. Besides the coloron, there are three physical spin-0 particles [2]: a color-octet, Θ , and two singlets, ϕ_I and ϕ_R . The constraints on the latter, which is a radial mode, have been derived in [12, 13] based on Higgs measurements, direct searches at the LHC, and electroweak observables. The processes discussed in Ref. [2] rely on the existence of a vector-like quark, which is not part of the minimal structure of the ReCoM.

In this paper, we systematically study the novel collider signatures in the ReCoM and point out new search strategies for discovering the coloron and the associated scalars. The color-octet scalar and ϕ_I are pseudo-Nambu-Goldstone bosons (pNGB's), and thus are naturally lighter than the coloron. Depending on the scalar masses and on the amount of mixing of the $SU(3)_1 \times SU(3)_2$ gauge bosons, the main decay channel of the coloron could be either $G'_\mu \rightarrow \Theta\phi_I$ or $\Theta\Theta$, while the dijet branching fraction may be below 10%.

The Θ and ϕ_I scalars have competing multi-body or multi-loop decays, as well as cascade decays in association with SM quark-antiquark pairs. As a result, the coloron appears as an s -channel multi-jet resonance, with two or more jet sub-clusters, and a total jet multiplicity as high as 12 when there are no top quarks produced. Channels that include $t\bar{t}$ pairs have even more complicated final states. For a lighter ϕ_I , below around 1 TeV, its main decay channels are into two electroweak gauge bosons. The collider signatures in that case include boosted W^+W^- , γZ or ZZ resonances, which typically originate from displaced vertices, plus a number of prompt quark jets or $t\bar{t}$ pairs. Currently, there are no dedicated searches at the LHC for these classes of signatures. The ReCoM thus provides a motivation for new searches at the LHC with complicated hadronic final states, various boosted systems, and displaced vertices.

The paper is organized as follows. We first work out the properties of the scalars in the ReCoM including their interactions and branching fractions in Section 2. In Section 3, we calculate the production cross sections in phenomenologically relevant channels. In Section 4, we identify the LHC signatures for different mass spectra and comment on search strategies. Our conclusions and two tables that summarize the main collider signatures are included in Section 5. In the Appendix, we derive the constraints on the scalar masses imposed by the condition that the color-conserving vacuum is the global minimum of the potential.

2 Renormalizable $SU(3)_1 \times SU(3)_2$ model

We study a gauge extension of the SM with an $SU(3)_1 \times SU(3)_2 \times SU(2)_W \times U(1)_Y$ gauge group and a new scalar field Σ transforming in the $(3, \bar{3}, 1, 0)$ representation. The most general renormalizable potential that involves only Σ has four terms:

$$V(\Sigma) = -m_\Sigma^2 \text{Tr}(\Sigma\Sigma^\dagger) - (\mu_\Sigma \det \Sigma + \text{H.c.}) + \frac{\lambda}{2} [\text{Tr}(\Sigma\Sigma^\dagger)]^2 + \frac{\kappa}{2} \text{Tr}(\Sigma\Sigma^\dagger\Sigma\Sigma^\dagger) . \quad (2.1)$$

The squared-mass parameter m_Σ^2 can be positive or negative. The phase-rotation freedom of Σ allows us to choose the mass parameter μ_Σ to be real and positive without loss of generality. At least one of the dimensionless couplings λ and κ must be positive. If one of them is negative, then the potential is bounded from below only when both $\lambda + \kappa$ and $3\lambda + \kappa$ are positive [11].

At the renormalizable level, there is also a potential term for Σ coupling to the SM Higgs doublet: $\text{Tr}(\Sigma\Sigma^\dagger)HH^\dagger$, which modifies the Higgs boson properties [12, 13]. In the following, we will assume a small coupling for this interaction so that the modifications to the Higgs boson properties are below the current experimental sensitivity.

2.1 Bosonic mass spectrum

As studied in detail in Ref. [11] (see also [14, 15]), and depending on the values of the four parameters in Eq. (2.1), there are three possible vacua with the gauge symmetries given by the diagonal subgroup $SU(3)_c$, or $SU(2)_1 \times SU(2)_2 \times U(1)$, or the full $SU(3)_1 \times SU(3)_2$. In ReCoM the phenomenologically viable regions of parameter space are those where the global minimum has the $SU(3)_c$ symmetry, identified with the QCD gauge group. These regions of parameter space are summarized in the Appendix.

The Σ field is a 3×3 matrix with complex entries, and its VEV is

$$\langle \Sigma \rangle = \frac{f_\Sigma}{\sqrt{6}} \mathbb{I}_3 \quad , \quad (2.2)$$

with \mathbb{I}_3 the unit matrix, and the scale of $SU(3)_1 \times SU(3)_2$ breaking given by

$$f_\Sigma = \frac{\sqrt{3}}{\sqrt{2}(3\lambda + \kappa)} \left(\sqrt{4(3\lambda + \kappa)m_\Sigma^2 + \mu_\Sigma^2} + \mu_\Sigma \right) > 0 \quad . \quad (2.3)$$

Eight of the degrees of freedom in Σ become the longitudinal degrees of freedom of the heavy gauge boson (the coloron), while the remaining ten degrees of freedom form a color-octet real scalar, Θ^a , and two singlet real scalars, ϕ_R and ϕ_I . The relation between these physical states and the uneaten degrees of freedom in Σ is

$$\Sigma = \frac{f_\Sigma + \phi_R + i\phi_I}{\sqrt{6}} \mathbb{I}_3 + \Theta^a T^a \quad , \quad (2.4)$$

where T^a are the $SU(3)_c$ generators, normalized as $\text{Tr}(T^a T^b) = \frac{1}{2} \delta^{ab}$. Since the new scalars in the ReCoM do not have tree-level couplings to fermions, they are \mathcal{P} -even. Under charge conjugation the scalars transform as $\Sigma \xrightarrow{\mathcal{C}} \Sigma^*$, which implies $\Theta^a T^a \xrightarrow{\mathcal{C}} \Theta^a (T^a)^*$, $\phi_R \xrightarrow{\mathcal{C}} \phi_R$, and $\phi_I \xrightarrow{\mathcal{C}} -\phi_I$. Thus, ϕ_I is a \mathcal{CP} -odd scalar which is also \mathcal{C} -odd. Its \mathcal{CP} property will determine its couplings to SM particles and lifetime, which will be discussed later. The squared-masses of the three scalar particles are given by

$$\begin{aligned} M_\Theta^2 &= \frac{\kappa}{3} f_\Sigma^2 + \sqrt{\frac{2}{3}} \mu_\Sigma f_\Sigma \quad , \\ M_{\phi_I}^2 &= \sqrt{\frac{3}{2}} \mu_\Sigma f_\Sigma \quad , \\ M_{\phi_R}^2 &= \left(\lambda + \frac{\kappa}{3} \right) f_\Sigma^2 - \frac{\mu_\Sigma}{\sqrt{6}} f_\Sigma \quad . \end{aligned} \tag{2.5}$$

Imposing that the $SU(3)_c$ -preserving vacuum is the global minimum of the potential, we prove in the Appendix that there is an upper bound for the ratio of the ϕ_I and Θ masses: $M_{\phi_I}/M_\Theta < 2.1$. In the limit of $\mu_\Sigma \ll f_\Sigma$, we have $M_{\phi_I} \ll M_{\phi_R}, M_\Theta$, indicating that the color-singlet scalar ϕ_I becomes the light pNGB associated with the spontaneous breaking of a global $U(1)_\Sigma$ symmetry acting on Σ . The other color-singlet scalar ϕ_R has a mass of order $\sqrt{\lambda + \kappa/3} f_\Sigma$, unless a fine-tuning of parameters makes it much lighter.

The limit of $\kappa \ll 1$ and $\mu_\Sigma \ll f_\Sigma$ is also interesting, as it enhances the global symmetry of the potential to $SO(18)$, which is the symmetry that rotates the degrees of freedom of Σ . This symmetry is spontaneously broken down to $SO(17)$ by $\langle \Sigma \rangle$, so that there are 17 light pNGB's in this case, which are the degrees of freedom within the longitudinal coloron, the color-octet scalar Θ , and ϕ_I . In that limit both Θ and ϕ_I are naturally lighter than the coloron and ϕ_R .

Let us label the $SU(3)_1 \times SU(3)_2$ gauge bosons by G_1 and G_2 , and the corresponding gauge couplings by h_1 and h_2 . One linear combination of the gauge bosons becomes the massless QCD gluon (G) and the orthogonal combination is massive, the coloron (G'):

$$\begin{aligned} G^\mu &= G_1^\mu \cos \theta + G_2^\mu \sin \theta \quad , \\ G'^\mu &= G_1^\mu \sin \theta - G_2^\mu \cos \theta \quad , \end{aligned} \tag{2.6}$$

where the mixing angle satisfies

$$\tan \theta = \frac{h_1}{h_2} \quad . \tag{2.7}$$

The QCD gauge coupling is related to the $SU(3)_1 \times SU(3)_2$ couplings by

$$g_s = \frac{h_1 h_2}{\sqrt{h_1^2 + h_2^2}} \quad , \tag{2.8}$$

and the coloron mass is

$$M_{G'} = \frac{g_s}{\sqrt{6}} \left(\tan \theta + \frac{1}{\tan \theta} \right) f_\Sigma \quad . \quad (2.9)$$

The gauge couplings are perturbative provided $3h_i^2/(16\pi^2) \lesssim 1$, based on naive dimensional analysis. These upper limits together with Eq. (2.8) translate into a constraint on $\tan \theta$: $0.15 \lesssim \tan \theta \lesssim 6.7$. We will use this range of $\tan \theta$ for our phenomenological analysis. We point out, however, that the tree-level analysis is more under control if the upper limit on the gauge couplings is lowered, *e.g.* $3h_i^2/(16\pi^2) \lesssim 1/3$, which gives $0.25 \lesssim \tan \theta \lesssim 4$.

2.2 Interactions of the new bosons

The interactions among physical scalars include a trilinear Θ term,

$$\bar{\mu}_\Sigma d^{abc} \Theta^a \Theta^b \Theta^c \quad , \quad (2.10)$$

where d^{abc} is the totally-symmetric color tensor. The coefficient $\bar{\mu}_\Sigma$ has mass dimension one, and receives contributions from the trilinear term in the $V(\Sigma)$ potential as well as from a quartic term in $V(\Sigma)$ with one insertion of the Σ VEV:

$$\begin{aligned} \bar{\mu}_\Sigma &= \sqrt{\frac{3}{2}} \kappa f_\Sigma - \mu_\Sigma \\ &= \frac{3g_s(1+\tan^2\theta)}{2M_{G'}\tan\theta} \left(M_\Theta^2 - \frac{8}{9} M_{\phi_I}^2 \right) \quad , \end{aligned} \quad (2.11)$$

where in the second line we have used the relations between parameters and boson masses from Eqs. (2.5) and (2.9). There are also trilinear interactions involving one ϕ_R singlet and either two color-octets or two ϕ_I singlets,

$$\frac{1}{2} \left[(\lambda + \kappa) f_\Sigma + \frac{\mu_\Sigma}{\sqrt{6}} \right] \phi_R \Theta^a \Theta^a + \frac{1}{2} \left[\left(\lambda + \frac{\kappa}{3} \right) f_\Sigma + \frac{2\mu_\Sigma}{\sqrt{6}} \right] \phi_R \phi_I^2 \quad . \quad (2.12)$$

The only other trilinear scalar interaction involves three ϕ_R and is less phenomenologically important.

The interactions of a single coloron with scalars are given by

$$\frac{g_s}{\tan \theta} G'_\mu{}^a \left[\frac{1}{\sqrt{6}} (1 + \tan^2 \theta) (\phi_I \partial^\mu \Theta^a - \Theta^a \partial^\mu \phi_I) - \frac{1}{2} (1 - \tan^2 \theta) f^{abc} \Theta^b \partial^\mu \Theta^c \right] \quad , \quad (2.13)$$

where f^{abc} is the totally-antisymmetric color tensor. Note that, for $\tan \theta = 1$, the coupling of G'_μ to two Θ 's vanishes. This is because when $h_1 = h_2$ [see Eq. (2.7)] there is an interchanging \mathcal{Z}_2 symmetry, under which $G_1^\mu \leftrightarrow G_2^\mu$, $G_\mu \leftrightarrow G_\mu$, $G'_\mu \leftrightarrow -G'_\mu$, $\Sigma \rightarrow \Sigma^\dagger$, $\phi_I \rightarrow -\phi_I$ and $\Theta^a \rightarrow \Theta^a$.

The couplings of a pair of colorons to a single scalar are

$$\frac{M_{G'}^2}{f_\Sigma} \left(\sqrt{\frac{3}{2}} d^{abc} G_\mu'^a G'^{\mu b} \Theta^c + G_\mu'^a G'^{\mu a} \phi_R \right). \quad (2.14)$$

We will not display here the interactions of two colorons with two scalars, the quartic scalar interactions, or the coloron self-interactions (the latter are important if one of the h_i gauge couplings is nearly nonperturbative).

For coloron interactions with fermions, we choose the simplest and anomaly-free model with the SM quarks as triplets under $SU(3)_1$ and singlets under $SU(3)_2$. The coloron interactions with quarks are flavor-blind and have the same form as those of the gluon, with an extra factor of $\tan \theta$:

$$g_s \tan \theta \bar{q} \gamma^\mu T^a G_\mu'^a q \quad . \quad (2.15)$$

2.3 Partial widths of the color-octet bosons

At tree-level and for $M_\Theta < M_{G'}$, the main decay of the color-octet scalar is into two quark-antiquark pairs, via two off-shell colorons: $\Theta \rightarrow G'^* G'^* \rightarrow q \bar{q} q' \bar{q}'$. Using Eqs. (2.14) and (2.9), the 4-body width to leading order in $M_\Theta^2 \ll M_{G'}^2$ is parametrically of the order of

$$\Gamma(\Theta \rightarrow q \bar{q} q' \bar{q}') \sim \frac{\alpha_s^3}{\pi^2} \tan^2 \theta (1 + \tan^2 \theta)^2 \frac{M_\Theta^7}{M_{G'}^6}, \quad (2.16)$$

where the width is summed over the quark flavors, and α_s is the QCD coupling constant. We have assumed here that the phase-space suppression is of the order of $(4\pi)^5$. For $M_\Theta \sim 1$ TeV, $M_{G'} \sim 4$ TeV and $\tan \theta \sim 0.3$, the 4-body width is at the keV scale. For larger M_Θ , of order $M_{G'}/2$, $\Gamma(\Theta \rightarrow q \bar{q} q' \bar{q}')$ is larger by a few orders of magnitude.

At one loop, Θ decays into two gluons. The amplitude for this process gets two contributions. The first one is from diagrams with Θ running in the loop and a vertex involving the trilinear interaction (2.10). The second contribution is from diagrams with the coloron running in the loop and the $G' G' \Theta$ vertex given in Eq. (2.14). Adding the two contributions, we have the following effective interaction:

$$\frac{C_\Theta}{f_\Sigma} \left(\frac{g_s^2}{16\pi^2} \right) d^{abc} \Theta^a G_{\alpha\beta}^b G^{c\alpha\beta}, \quad (2.17)$$

where the dimensionless coefficient is

$$C_\Theta = 6\sqrt{2} \left(\frac{\pi^2}{9} - 1 \right) \frac{\bar{\mu}_\Sigma f_\Sigma}{M_\Theta^2} + \frac{3\sqrt{6}}{32} \mathcal{A}[M_\Theta^2/(4M_{G'}^2)] \quad . \quad (2.18)$$

Here, the function $\mathcal{A}(\tau) = [2\tau^2 + 3\tau + 3(2\tau - 1) \arcsin^2 \sqrt{\tau}] \tau^{-2}$ for $\tau \leq 1$, which is similar to the W^\pm loop contributions to the effective interaction of the Higgs boson with two photons. In the $\tau \rightarrow 0$ limit, the function $\mathcal{A}(\tau)$ reaches its minimum, $\mathcal{A}(0_+) \rightarrow 7$; $\mathcal{A}(\tau)$

increases monotonically with τ , and $A(1/4) \approx 7.42$. The ratio of the second term to the first term in Eq. (2.18) has a simple formula:

$$\begin{aligned} r_{\mathcal{A}} &= \frac{3}{32\sqrt{2}(\pi^2 - 9)} \frac{\mathcal{A}[M_{\Theta}^2/(4M_{G'}^2)]}{1 - 8M_{\phi_I}^2/(9M_{\Theta}^2)} \\ &\approx 0.533 \left(1 + \frac{8M_{\phi_I}^2}{9M_{\Theta}^2} + \frac{11M_{\Theta}^2}{210M_{G'}^2} + \dots \right), \end{aligned} \quad (2.19)$$

where the ellipsis in the second line refers to higher-order terms in $M_{\phi_I}^2/M_{\Theta}^2$ and $M_{\Theta}^2/M_{G'}^2$. The above expression shows that the two contributions to $\Theta \rightarrow gg$ are comparable. Using the result for the scalar contribution given in [2], and including the interference with the coloron contribution, we find the $\Theta \rightarrow gg$ width:

$$\begin{aligned} \Gamma(\Theta \rightarrow gg) &= \frac{15\alpha_s^2 \bar{\mu}_{\Sigma}^2}{128\pi^3 M_{\Theta}} \left(\frac{\pi^2}{9} - 1 \right)^2 (1 + r_{\mathcal{A}})^2 \\ &\approx \frac{135\alpha_s^2}{256\pi^3} \left(\frac{\pi^2}{9} - 1 \right)^2 (1 + r_{\mathcal{A}})^2 \kappa M_{\Theta}, \end{aligned} \quad (2.20)$$

where the approximation in the second line is taken in the limit of $\mu_{\Sigma} \ll \kappa f_{\Sigma}$ (which implies $M_{\phi_I} \ll M_{\Theta}$). Note the accidental suppression of the above width by a factor of $(\pi^2/9 - 1)^2 \approx 9.3 \times 10^{-3}$. The interference of the scalar and coloron contributions is constructive for $M_{\phi_I} < 6\sqrt{2} M_{\Theta}$, which is automatically satisfied in the ReCoM (see the Appendix). For $M_{\Theta} = 1$ TeV, $M_{G'} = 4$ TeV, $M_{\phi_I} = 300$ GeV and $\tan\theta \sim 0.3$, the 1-loop 2-body width of Θ is around 2 MeV, much above the tree-level 4-body one.

We also note that there is an effective interaction of Θ^a with two quarks, which can be generated at one loop, with a G' and a quark running in the loop. However, this scalar-fermion interaction is suppressed by the ratio of fermion mass over coloron mass. Even for the top quark, the estimated width is smaller by two orders of magnitude than the one of $\Theta \rightarrow gg$. We will ignore this small branching fraction in our analysis.

If $M_{\Theta} > M_{\phi_I}$, then Θ also has 3-body tree-level decays into a ϕ_I scalar and a quark-antiquark pair of same flavor, $\Theta \rightarrow \bar{q}q\phi_I$, through an off-shell G' . Neglecting the quark masses, the partial widths of Θ into a ϕ_I and either a pair of quark jets (jj) or $t\bar{t}$ satisfy

$$\Gamma(\Theta \rightarrow jj\phi_I) \simeq 5\Gamma(\Theta \rightarrow t\bar{t}\phi_I) \simeq \frac{5\alpha_s^2 M_{\Theta}^5}{576\pi M_{G'}^4} (1 + \tan^2\theta)^2 \mathcal{F}(M_{\Theta}^2/M_{G'}^2, M_{\phi_I}^2/M_{G'}^2), \quad (2.21)$$

where we defined the function

$$\begin{aligned} \mathcal{F}(x, y) &= \frac{12}{x^4} \left[(y-x) \left(1 - \frac{3}{2}(x+y) + \frac{1}{3}(x-y)^2 \right) + \frac{1}{2} \left(1 - 2(x+y) + x^2 + y^2 \right) \log\left(\frac{x}{y}\right) \right. \\ &\quad \left. + (1-x-y) \left(1 - 2(x+y) + (x-y)^2 \right)^{1/2} \tanh^{-1} \left(\frac{(1 - 2(x+y) + (x-y)^2)^{1/2}}{x - y - (x+y)/(x-y)} \right) \right]. \end{aligned} \quad (2.22)$$

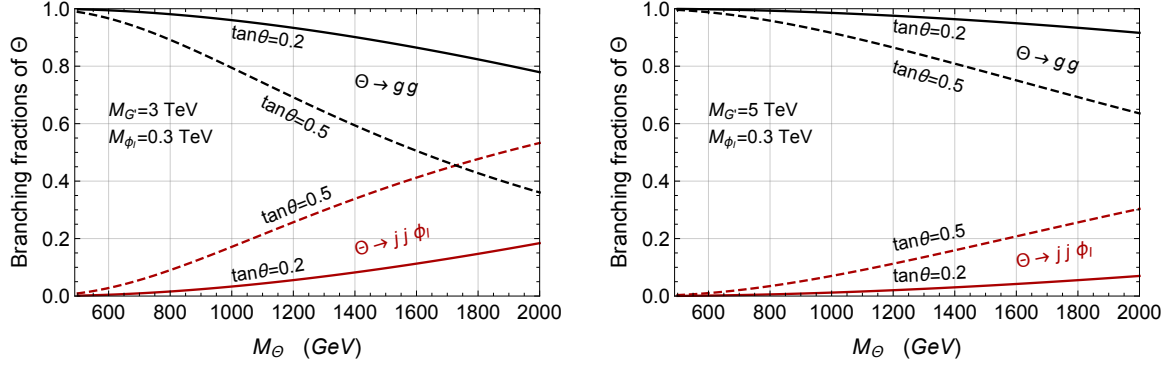


Figure 1: Branching fractions of the color-octet scalar Θ as a function of its mass. For $\Theta \rightarrow jj\phi_I$ the width is summed over the five light quark flavors in the final state. The branching fraction for $\Theta \rightarrow t\bar{t}\phi_I$ (not shown) is slightly less than $1/5$ of that for $\Theta \rightarrow jj\phi_I$. The coloron mass used here is $M_{G'} = 3$ TeV (left panel) or 5 TeV (right panel), and the neutral scalar mass is fixed at $M_{\phi_I} = 300$ GeV. The parameter $\tan\theta$, which determines the strength of the coloron couplings, is taken to be 0.2 (solid lines) or 0.5 (dashed lines).

In Figure 1, we show the branching fractions of 2- and 3-body decays as a function of M_Θ for fixed masses of ϕ_I and the coloron. Note that the 3-body branching fraction increases as M_Θ increases. For a fixed value of M_Θ , increasing the mixing parameter $\tan\theta$ leads to an increase of the 3-body branching fraction. It is helpful to take the $M_\Theta, M_{\phi_I} \ll M_{G'}$ limit (for any $M_\Theta > M_{\phi_I}$) in Eq. (2.21), which corresponds to the following limit:

$$\mathcal{F}(x, y) \xrightarrow{x, y \ll 1} 1 - 8\frac{y}{x} + 12\frac{y^2}{x^2} \log\left(\frac{x}{y}\right) + 8\frac{y^3}{x^3} - \frac{y^4}{x^4} . \quad (2.23)$$

The coloron with a mass above the scalar pair thresholds, ($M_{G'} > M_\Theta + M_{\phi_I}, 2M_\Theta$) has four 2-body decay channels with widths [2]

$$\begin{aligned} \Gamma(G'_\mu \rightarrow \Theta \phi_I) &\approx \frac{\alpha_s}{72 \tan^2\theta} (1 + \tan^2\theta)^2 M_{G'} , \\ \Gamma(G'_\mu \rightarrow \Theta \Theta) &\approx \frac{\alpha_s}{64 \tan^2\theta} (1 - \tan^2\theta)^2 M_{G'} , \\ \Gamma(G'_\mu \rightarrow jj) &\approx 5 \Gamma(G'_\mu \rightarrow t\bar{t}) \approx \frac{5\alpha_s}{6} \tan^2\theta M_{G'} , \end{aligned} \quad (2.24)$$

where we have ignored the phase-space suppression due to final-state particle masses (we will include them later in the numerical calculation). In Figure 2, we show the branching fractions of G' as a function of $M_{G'}$. For $\tan\theta$ larger than about 0.45 (as in the right-hand panel), the decays of G' are dominated by the dijet channel, while for a smaller value of $\tan\theta$ (as in the left-hand panel), the decays into $\Theta\phi_I$ and $\Theta\Theta$ have large branching fractions.

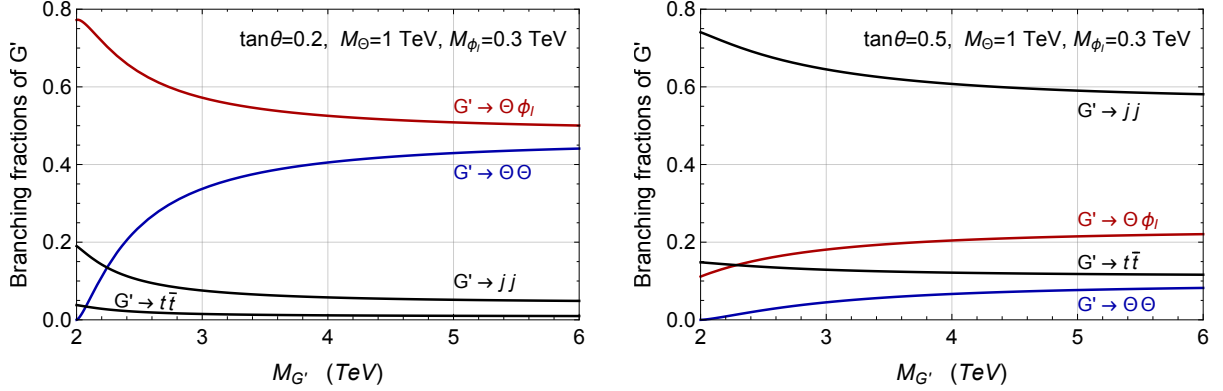


Figure 2: Branching fractions of the coloron, G' , as a function of its mass, for $\tan \theta = 0.2$ (left panel) or $\tan \theta = 0.5$ (right panel). The scalar masses are fixed at $M_\Theta = 1$ TeV and $M_{\phi_I} = 300$ GeV.

2.4 Partial widths of the singlet scalar ϕ_I

The main decay channel of the ϕ_I scalar, in the case of the $M_{\phi_I} > M_\Theta$ mass ordering, is a 3-body one: $\phi_I \rightarrow jj \Theta$ via an off-shell G' with a width

$$\Gamma(\phi_I \rightarrow jj \Theta) \simeq 5 \Gamma(\phi_I \rightarrow t \bar{t} \Theta) \approx \frac{5 \alpha_s^2 M_{\phi_I}^5}{72 \pi M_{G'}^4} (1 + \tan^2 \theta)^2 \mathcal{F}(M_{\phi_I}^2/M_{G'}^2, M_\Theta^2/M_{G'}^2), \quad (2.25)$$

where the function $\mathcal{F}(x, y)$ is defined in Eq. (2.22). Comparing Eqs. (2.21) and (2.25), note that the order of M_Θ and M_{ϕ_I} is reversed in the arguments of \mathcal{F} .

In the case of the other mass ordering, $M_{\phi_I} < M_\Theta$, the leading decay of ϕ_I is likely to be a 4-body one into two gluons plus two quarks via the diagrams shown in Figure 3. The first diagram there is the decay via an off-shell G' and an off-shell Θ . Note that the Θ coupling to a gluon pair arises at one loop, and is described by the dimension-5 operator (2.17), with the coefficient C_Θ defined in Eq. (2.18). Extracting f_Σ from Eq. (2.9), and using the expressions for $\bar{\mu}_\Sigma$ and r_A given in Eqs. (2.11) and (2.19), we find

$$C_\Theta \approx 4.61 \left(1 - 0.58 \frac{M_{\phi_I}^2}{M_\Theta^2} + 0.018 \frac{M_\Theta^2}{M_{G'}^2} + \dots \right), \quad (2.26)$$

where higher-order terms in $M_{\phi_I}^2/M_\Theta^2$ and $M_\Theta^2/M_{G'}^2$ are represented by the dots. The effective coupling of ϕ_I to gluons and quarks induced by the first diagram in Figure 3 is described in the $M_{\phi_I}^2 \ll M_\Theta^2, M_{G'}^2$ limit by a dimension-9 operator:

$$C_\Theta \frac{g_s^3 \tan \theta}{32 \pi^2 f_\Sigma^2 M_{G'} M_\Theta^2} d^{abc} (\partial_\mu \phi_I) \bar{q} \gamma^\mu T^a q G_{\alpha\beta}^b G^{c\alpha\beta}. \quad (2.27)$$

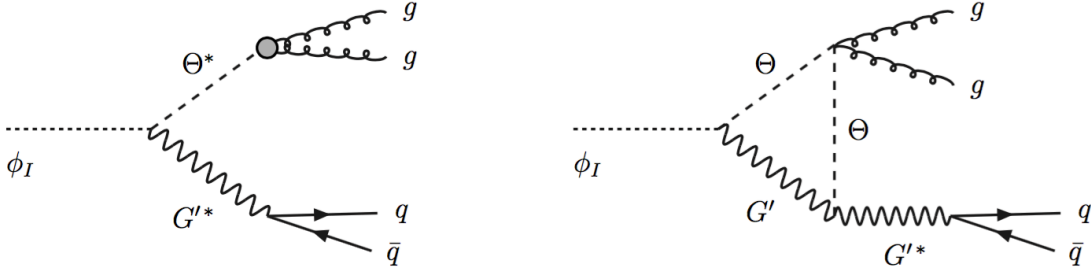


Figure 3: Diagrams responsible for the 4-body decay $\phi_I \rightarrow g g q \bar{q}$ of the \mathcal{CP} -odd scalar when $M_{\phi_I} < M_\Theta$. Left diagram: decay through an off-shell coloron and an off-shell Θ scalar, which couples at one loop to two gluons. Right diagram: 1-loop decay into a gluon pair and an off-shell coloron (other ways of attaching the gluons to the loop are not shown). The coloron interactions with scalars are given in Eq. (2.13).

The second diagram shown in Figure 3, together with four similar 1-loop diagrams where the two gluons are attached in different ways to the Θ and G' internal lines, contribute to the same operator (for $M_{\phi_I}^2 \ll M_\Theta^2$), as well as to other dimension-9 operators with different Lorentz contractions. All these contributions are parametrically of the same order. Assuming that ϕ_I is much heavier than the QCD scale (so we do not need to take into account hadronization effects), the 4-body width of ϕ_I summed over 5 light quark flavors can be written as

$$\begin{aligned} \Gamma(\phi_I \rightarrow g g q \bar{q}) &= \frac{2}{189 (4\pi)^5} (C_\Theta + C'_\Theta)^2 \left(\frac{g_s^3 \tan \theta}{32\pi^2 f_\Sigma^2 M_{G'} M_\Theta^2} \right)^2 M_{\phi_I}^{11}, \\ &= \frac{\alpha_s^5}{168 (12\pi)^4} (C_\Theta + C'_\Theta)^2 \frac{(1 + \tan^2 \theta)^4}{\tan^2 \theta} \frac{M_{\phi_I}^{11}}{M_\Theta^4 M_{G'}^6}, \end{aligned} \quad (2.28)$$

where C'_Θ is a function of $M_\Theta/M_{G'}$ that takes into account the 1-loop diagrams of the type shown on the right-hand side of Figure 3. We expect that C'_Θ is typically of order one or smaller. There is also a $\phi_I \rightarrow g g t \bar{t}$ decay, whose width is smaller by a factor of 5 (or more when M_{ϕ_I} is not much larger than $2m_t$). For $M_{\phi_I} = 700$ GeV, $M_\Theta = 1$ TeV, $M_{G'} = 3$ TeV and $\tan \theta = 0.3$, the width of ϕ_I is of the order of 5×10^{-13} GeV, corresponding to a lifetime $\tau_{\phi_I}^0 \approx 10^{-12}$ s. Note that the lifetime is proportional to $M_{\phi_I}^{-11}$. Thus, a lighter ϕ_I produced at the LHC can easily have a long displaced vertex if the 4-body decay is the dominant channel. In Section 4.2 we will estimate the ϕ_I decay length in the lab frame.

One may wonder about 2-body decay channels like $\phi_I \rightarrow g g$, as in the case of Θ discussed earlier (see Section 2.3). As pointed out below Eq. (2.4), the ϕ_I is a \mathcal{C} -odd and \mathcal{P} -even scalar. Its decay into two gluons is therefore highly suppressed by charge-conjugation symmetry, requiring electroweak interactions, which enter only at four loops. That symmetry will not forbid ϕ_I decays into three gluons. The lowest-dimension operator appears to be $\phi_I d^{abc} G_\nu^{a\mu} G_\mu^{b\alpha} G_\alpha^{c\nu}$, but this operator vanishes because the gluon field

strength is antisymmetric in Lorentz indices. The next operators are at dimension 9, containing $d^{abc} (\partial_\mu \phi_I) (D_\nu G^{a\mu\nu}) G_{\alpha\beta}^b G^{c\alpha\beta}$, and has the same structure as the one in Eq. (2.27) after using the field equation for the gluon.

Another possible decay of ϕ_I is into a quark-antiquark pair, with or without one more boson. To conserve \mathcal{C} , the effective operator below electroweak symmetry breaking is $(\partial_\mu \phi_I) \bar{t} \gamma^\mu t$, which is zero after using the fermion equation of motion. The next non-vanishing operator is at dimension 7, $(\partial_\mu \phi_I) H H^\dagger \bar{t} \gamma^\mu t$, where H is the Higgs doublet. This includes the non-vanishing interaction $\phi_I (\partial_\mu h^0) \bar{t} \gamma^\mu t$, where h^0 is the SM Higgs boson. This interaction can be generated by a 2-loop diagram (see the left panel of Figure 4), with Θ and G' running in the loop, and can be written as

$$\eta_1 (M_\Theta / M_{G'}) \tan \theta (1 + \tan^2 \theta)^2 \frac{10\sqrt{2} g_s^5 y_t^2 v_{\text{EW}}}{9(16\pi^2)^2 M_{G'}^3} \phi_I (\partial_\mu h^0) \bar{t} \gamma^\mu t . \quad (2.29)$$

Here, $v_{\text{EW}} \approx 246$ GeV is the Higgs VEV; y_t is the top quark Yukawa coupling; η_1 is a dimensionless coefficient which we expect to be of order one, or slightly smaller; the factor $10/9$ comes from color contractions. For $M_{\phi_I} > m_h + 2m_t \approx 470$ GeV and ignoring the final state phase-space factor, the 3-body decay width is calculated to be

$$\Gamma(\phi_I \rightarrow h^0 t \bar{t}) \simeq \frac{25 \alpha_s^5 \eta_1^2 y_t^4}{162 (4\pi)^6} \tan^2 \theta (1 + \tan^2 \theta)^4 \frac{v_{\text{EW}}^2 M_{\phi_I}^5}{M_{G'}^6} . \quad (2.30)$$

The decays into lighter quarks are further suppressed by small Yukawa couplings and are negligible. Combining (2.28) and (2.30), the ratio of the 2-loop 3-body and 1-loop 4-body decays of ϕ_I is

$$\frac{\Gamma(\phi_I \rightarrow h^0 t \bar{t})}{\Gamma(\phi_I \rightarrow g g q \bar{q})} \approx 2.6 \times 10^{-3} \eta_1^2 \left(\frac{\tan \theta}{0.3} \right)^4 \left(\frac{M_\Theta}{1 \text{ TeV}} \right)^4 \left(\frac{700 \text{ GeV}}{M_{\phi_I}} \right)^6 . \quad (2.31)$$

Hence, the 2-loop 3-body decay could be relevant only for a small M_{ϕ_I} , below around 300 GeV, in which case the collider signature involves a displaced vertex.

As both \mathcal{C} and \mathcal{P} are explicitly broken by the electroweak interactions, there are more \mathcal{C} and \mathcal{P} -violating operators for ϕ_I decaying into SM particles. At the 2-loop level, a Feynman diagram similar to the one on the left side of Figure 4, with h^0 replaced by the hypercharge gauge boson B_μ , generates the following representative dimension-7 operator:

$$\eta_2 (M_\Theta / M_{G'}) \tan \theta (1 + \tan^2 \theta)^2 \frac{5 g_s^5 e}{9 (16\pi^2)^2 c_W M_{G'}^3} (\partial^\mu \phi_I) \bar{q} \gamma^\nu \gamma_5 q B_{\mu\nu} , \quad (2.32)$$

where η_2 is a coefficient of order one or smaller, and c_W is the cosine of the weak mixing angle. The ensuing 2-loop 3-body decays, involving a photon or a Z boson, have a width

$$\Gamma(\phi_I \rightarrow \gamma q \bar{q}) \simeq \frac{c_W^2}{s_W^2} \Gamma(\phi_I \rightarrow Z q \bar{q}) \simeq \frac{5 \alpha \alpha_s^5 \eta_2^2}{648 (4\pi)^5} \tan^2 \theta (1 + \tan^2 \theta)^4 \frac{M_{\phi_I}^7}{M_{G'}^6} , \quad (2.33)$$

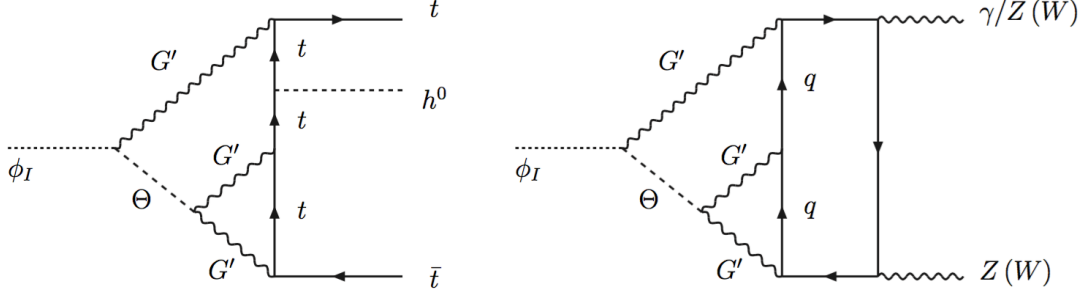


Figure 4: Additional decays of the \mathcal{CP} -odd scalar when $M_{\phi_I} < M_{\Theta}$. Left diagram: $\phi_I \rightarrow t\bar{t}h^0$ at two loops. Right diagram: $\phi_I \rightarrow \gamma Z, ZZ, W^+W^-$ at three loops.

where we ignored the final state particle masses, and summed over 5 quark flavors. The ratio of these 2-loop 3-body and the 1-loop 4-body widths of ϕ_I is

$$\frac{\Gamma(\phi_I \rightarrow \gamma/Z q \bar{q})}{\Gamma(\phi_I \rightarrow ggq\bar{q})} \approx 1.3 \times 10^{-4} \eta_2^2 \left(\frac{\tan \theta}{0.3} \right)^4 \left(\frac{M_{\Theta}}{1 \text{ TeV}} \right)^4 \left(\frac{700 \text{ GeV}}{M_{\phi_I}} \right)^4. \quad (2.34)$$

There are also decay channels involving the W boson, $\phi_I \rightarrow W^{\pm} q \bar{q}'$ with comparable branching fractions. Thus, the 2-loop 3-body widths with an electroweak boson in the final state are probably too small to be relevant for collider studies.

At the 3-loop level, ϕ_I couples to two electroweak bosons or two SM fermions. A diagram of this type is shown on the right-hand side of Figure 4. The \mathcal{CP} -conserving operators that couple the \mathcal{CP} -odd scalar to two electroweak gauge bosons include

$$\eta_3(M_{\Theta}/M_{G'}) \tan \theta (1 + \tan^2 \theta)^2 \frac{5 g_s^5 e^2}{2(16\pi^2)^3 M_{G'}} \phi_I \left(\frac{1}{s_W^2} W_{\mu\nu}^i \widetilde{W}^{i\mu\nu} - \frac{1}{c_W^2} B_{\mu\nu} \widetilde{B}^{\mu\nu} \right), \quad (2.35)$$

where η_3 again is a coefficient of order one or smaller, which depends on the ϕ_I , Θ and G' masses, and can be found by computing the 3-loops diagrams. The coefficient of the above operator for the hypercharge gauge boson includes a factor of $-3/2$, which accounts for the sum over the squared hypercharges of the six quark flavors running in the loop. The coefficient for the W^i gauge bosons comes from three generations of quarks and $1/2$ for the normalization of $SU(2)_W$ generators. The overall coefficient in (2.35) includes a color factor of $10/3$. Interestingly, after rotating the basis to γ , Z and W^{\pm} , there is no 3-loop coupling of ϕ_I to two photons. For other combinations of two gauge bosons, the 3-loop 2-body decays have widths

$$\begin{aligned} \Gamma(\phi_I \rightarrow \gamma Z) &\simeq \frac{s_W^2}{c_W^2} \Gamma(\phi_I \rightarrow W^+ W^-) \simeq \frac{2s_W^2 c_W^2}{1 - 4s_W^2 c_W^2} \Gamma(\phi_I \rightarrow ZZ) \\ &\simeq \frac{25 \alpha^2 \alpha_s^5 \eta_3^2}{2(4\pi)^6 s_W^2 c_W^2} \tan^2 \theta (1 + \tan^2 \theta)^4 \frac{M_{\phi_I}^3}{M_{G'}^2}. \end{aligned} \quad (2.36)$$

The ratios of these 3-loop 2-body widths to the 1-loop 4-body width of ϕ_I given in Eq. (2.28) are

$$\frac{\Gamma(\phi_I \rightarrow \gamma Z, WW, ZZ)}{\Gamma(\phi_I \rightarrow g g q \bar{q})} \approx (0.20, 0.66, 0.16) \eta_3^2 \left(\frac{\tan \theta}{0.3} \right)^4 \left(\frac{M_{G'}}{3 \text{ TeV}} \right)^4 \left(\frac{M_\Theta}{1 \text{ TeV}} \right)^4 \left(\frac{700 \text{ GeV}}{M_{\phi_I}} \right)^8. \quad (2.37)$$

If $\eta_3 = O(1)$, the 2-body decays into two electroweak bosons become the leading decay channels of ϕ_I for M_{ϕ_I} below around 700 GeV, or for $M_{G'} M_\Theta$ above 3 TeV². If η_3 turns out to be much smaller, $\eta_3^2 = O(10^{-3})$, then the 2-body decays become dominant for $M_{\phi_I} \lesssim 300$ GeV when $M_{G'} M_\Theta \sim 3$ TeV².

At the 3-loop level (*e.g.*, the left diagram of Figure 4 with an additional W loop attached to the top quark lines and no h^0), the \mathcal{CP} -conserving couplings to two fermions contain the dimension-5 operator

$$\eta_4(M_\Theta/M_{G'}) \tan \theta (1 + \tan^2 \theta)^2 \frac{5 g_s^5 e^2}{9(16\pi^2)^3 s_W^2 M_{G'}} (\partial_\mu \phi_I) \bar{t} \gamma^\mu \gamma_5 t. \quad (2.38)$$

After using integration by parts and fermion equation of motion, it is easy to show that the coupling is proportional to the fermion mass, so the top quark (if kinematically allowed) is the most important channel. Ignoring the final-state fermion masses, this 3-loop 2-body decay width is then

$$\Gamma(\phi_I \rightarrow t \bar{t}) \simeq \frac{25 \alpha^2 \alpha_s^5 \eta_4^2}{81(4\pi)^6 s_W^4} \tan^2 \theta (1 + \tan^2 \theta)^4 \frac{m_t^2 M_{\phi_I}}{M_{G'}^2}. \quad (2.39)$$

The ratio of this decay mode over the 1-loop 4-body one is

$$\frac{\Gamma(\phi_I \rightarrow t \bar{t})}{\Gamma(\phi_I \rightarrow g g q \bar{q})} \approx 1.0 \times 10^{-3} \eta_4^2 \left(\frac{\tan \theta}{0.3} \right)^4 \left(\frac{M_{G'}}{3 \text{ TeV}} \right)^4 \left(\frac{M_\Theta}{1 \text{ TeV}} \right)^4 \left(\frac{700 \text{ GeV}}{M_{\phi_I}} \right)^{10}. \quad (2.40)$$

Comparing the two 3-loop widths in (2.36) and (2.39), the fermion pair channel is suppressed by $m_t^2/M_{\phi_I}^2$ for comparable η_3 and η_4 .

In conclusion, for M_{ϕ_I} not dramatically below $M_{G'}$ and M_Θ , the main decay of ϕ_I is the 1-loop 4-body channel $\phi_I \rightarrow g g q \bar{q}$ in (2.28), otherwise the main channels appear to be $\phi_I \rightarrow \gamma Z, W^+ W^-, Z Z$ with the widths estimated in (2.36).

3 Production of scalars at the LHC

The ReCoM is a relatively simple gauge theory. It contains only four new particles beyond the SM: the spin-1 coloron, the color-octet scalar Θ , and two singlet scalars. Nevertheless, there are several processes at the LHC that lead to the production of these particles.

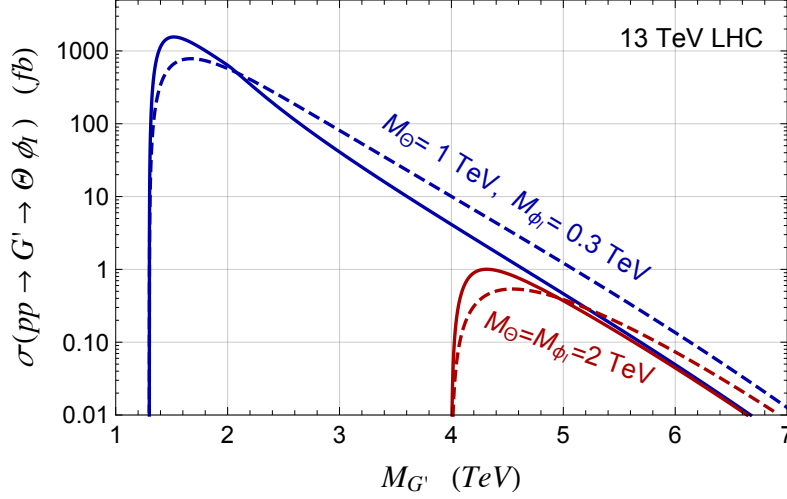


Figure 5: Cross section for the $pp \rightarrow G' \rightarrow \Theta \phi_I$ process at $\sqrt{s} = 13$ TeV as a function of the coloron mass for $\tan \theta = 0.2$ (solid lines) or 0.5 (dashed lines). The scalar masses are fixed at $M_\Theta = 1$ TeV and $M_{\phi_I} = 300$ GeV (blue lines), or at $M_\Theta = M_{\phi_I} = 2$ TeV (red lines).

A peculiar production process is $q\bar{q} \rightarrow G' \rightarrow \Theta \phi_I$, which is resonant production of two scalar particles of different masses and carrying different color charges. In the narrow width approximation, the tree-level G' parton-level production cross section is given by

$$\sigma(q\bar{q} \rightarrow G') \approx \frac{8\pi^2 \alpha_s \tan^2 \theta}{9M_{G'}} \delta(\sqrt{\hat{s}} - M_{G'}) . \quad (3.1)$$

Next-to-leading order corrections to coloron production have been computed in [16], and can be approximated by a multiplicative K -factor of about 1.2. At the 13 TeV LHC, the G' production cross section is approximately (20, 1.8, 0.20) pb for $M_{G'} = 2, 3, 4$ TeV. Using the MSTW parton distribution functions [17], $K = 1.2$, and the branching fraction for $G' \rightarrow \Theta \phi_I$ (see Figure 2), we find the cross section for $\Theta \phi_I$ production shown in Figure 5.

The color-octet scalar Θ can be pair-produced at hadron colliders through two very different processes. The first one, which we loosely refer to as QCD production, is due to the Θ coupling to the gluons, which is governed by the QCD gauge coupling $g_s = \sqrt{4\pi\alpha_s} \approx 1$ (here α_s is the strong coupling constant at a scale of order $2M_\Theta$). There are four types of Feynman diagrams that contribute to QCD production at leading order [2]: three diagrams from the gg initial state (via an s -channel gluon, a t -channel Θ , or a $gg\Theta\Theta$ coupling) and one diagram from $q\bar{q}$ initial states (via an s -channel gluon). At the LHC, the gluon-initiated processes have a rate larger than the $q\bar{q}$ ones, unless Θ is very heavy.

The second process that leads to Θ pair production involves an s -channel coloron. At leading order this is due to quark-antiquark initial states, so it interferes only with the

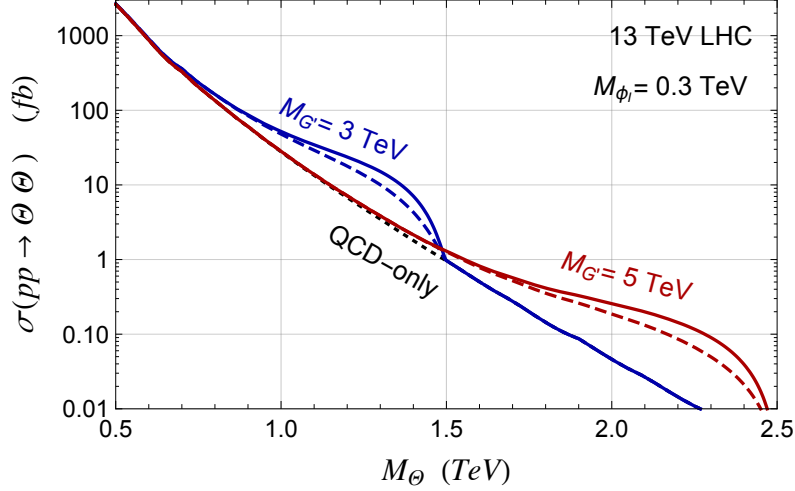


Figure 6: Leading-order cross section for $\Theta\Theta$ production (due to an s -channel G' , QCD and interference) at the 13 TeV LHC as a function of the Θ mass. The coloron mass is fixed at $M_{G'} = 3$ TeV (blue lines) or 5 TeV (red lines), while $\tan\theta = 0.2$ (solid lines) or 0.5 (dashed lines). The dependence on the neutral-scalar mass (fixed here at $M_{\phi_I} = 300$ GeV) is mild. The dotted line represents the QCD contribution.

$q\bar{q}$ -initiated QCD production. The total $\Theta\Theta$ production cross section at the 13 TeV LHC is shown in Figure 6 as a function of the Θ mass, for $M_{G'} = 3$ TeV or 5 TeV, $\tan\theta = 0.2$ or 0.5, and $M_{\phi_I} = 300$ GeV. The dependence on M_{ϕ_I} (due to the $G' \rightarrow \Theta\phi_I$ branching fraction) is negligible when this parameter is much smaller than M_Θ .

There are also two classic processes, $q\bar{q} \rightarrow G' \rightarrow jj$ and $q\bar{q} \rightarrow G' \rightarrow t\bar{t}$, which have been searched for by the ATLAS and CMS experiments, and can be used to exclude a certain region of the parameter space. After taking into account of the acceptance of around 0.6 [18], the CMS collaboration has set an upper constraint on the cross section times branching fraction (σB) from dijet resonance searches with 36 fb^{-1} of data (similar constraints are also imposed by the ATLAS collaboration [19]). For $M_{G'} = (2, 3, 4)$ TeV, the constraint is $\sigma(pp \rightarrow G')B(G' \rightarrow jj) \leq (100, 20, 10) \text{ fb}$ [18]. For a small mixing of $\tan\theta = 0.2$, $B(G' \rightarrow jj)$ could be as small as 0.1 such that the constraints on the coloron mass is around $M_{G'} \gtrsim 2$ TeV.

In Figure 7, we show the constraints on the mixing parameter $\tan\theta$ for different coloron masses from the dijet resonance searches. We also note that the $t\bar{t}$ resonance searches are less sensitive because of the smaller branching fraction [20]. It is clear from the left panel of Figure 2 that the main decay channels of the coloron for small $\tan\theta$ are into the scalars in the ReCoM, which provides novel signatures at the LHC and will be the focus of next section.

The second singlet scalar, ϕ_R , cannot be produced in coloron decays, as it only couples to $G'_\mu G'^\mu$. This coupling allows the non-resonant production of ϕ_R in association with a

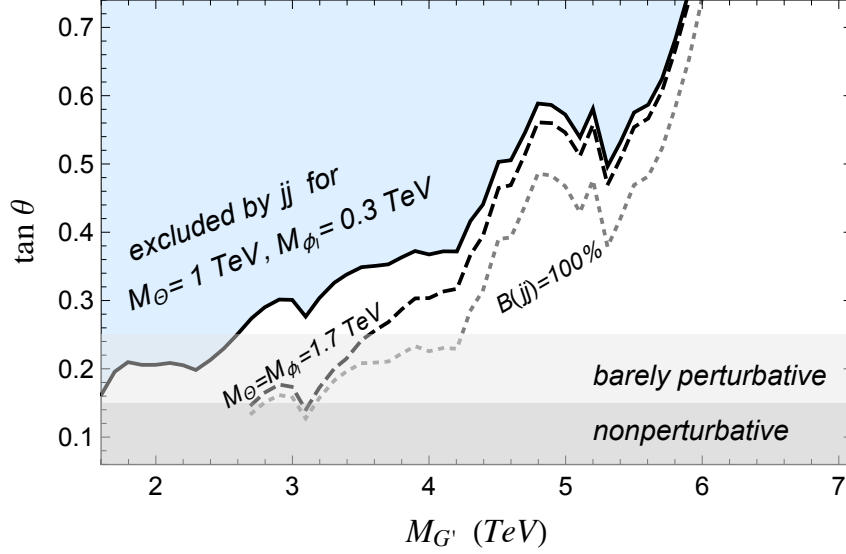


Figure 7: Excluded regions of the coloron parameter space. Region above solid black line is ruled out, for $M_\Theta = 1$ TeV and $M_{\phi_I} = 300$ GeV, by jj resonance searches, assuming that $pp \rightarrow G' \rightarrow jj$ is the only new-physics process contributing to the dijet final state. Similarly, the region above the dashed line is ruled out for $M_\Theta = M_{\phi_I} = 1.7$ TeV. The region above the dotted line is ruled out when the effective jj branching fraction is 100% (*e.g.*, scalar masses are above $M_{G'}/2$ and the boosted $t\bar{t}$ signal mimics a jj one). In the region labelled “barely perturbative”, the expansion parameter for loops that involve the coloron self-coupling is relatively large [$3h_2^2/(16\pi^2)$ between 1/3 and 1] so that the tree-level result is expected to get sizable corrections.

coloron. Single production of ϕ_R also proceeds through a gluon fusion process induced at one loop, with separate contributions from the coloron and the Θ scalar running in the loop. If ϕ_R is heavy enough, it can decay into a pair of ϕ_I or Θ scalars due to the trilinear couplings in Eq. (2.12). The ϕ_R scalar may also decay into pairs of heavy SM particles due to its mixing with the SM Higgs boson, as studied in [12, 13].

Another class of processes is based on coloron pair production through its gluon couplings. Even though this production is non-resonant and kinematically suppressed by the presence of two heavy colorons, its cross section relies solely on the QCD coupling and is above 1 fb for a coloron mass below about 2.5 TeV [21]. Depending on the decay channels, this may be large enough for the high-luminosity run of the LHC. The coloron decays into scalar pairs in this case leads to intermediate states involving 4Θ or $3\Theta + \phi_I$ or $\Theta\phi_I\Theta\phi_I$, which give rise to complicated final states with high jet multiplicity.

In the next section we will focus on the final states that arise from $\Theta\phi_I$ or $\Theta\Theta$ production, which have larger cross sections.

4 Novel LHC signatures

The ReCoM predicts rich collider phenomena with many complicated final states involving hadronic activity and other objects. At the LHC, the single production of Θ or ϕ_I is suppressed due to loop factors. Therefore, we will concentrate on the pair-productions $pp \rightarrow \Theta\Theta$ and $pp \rightarrow \Theta\phi_I$ and point out the novel signatures in the ReCoM.

To study the current experimental bounds and interesting signatures that have not been searched for at the LHC, we consider two types of mass orderings: $M_{G'} > M_{\phi_I} > M_\Theta$ and $M_{G'} > M_\Theta > M_{\phi_I}$. In the following, we will study the leading collider signatures for each case and point out the discovery potential.

4.1 Light color-octet scalar: $M_{G'} > M_{\phi_I} > M_\Theta$

For this parameter region, the color-octet scalar Θ mainly decays into two gluons ($\Theta \rightarrow gg$), while the singlet scalar predominantly decays via an off-shell coloron into a 3-body final state: $\phi_I \rightarrow jj\Theta$ with the two jets originating from quarks. After the subsequent Θ decaying to two gluons, ϕ_I behaves as a 4-jet resonance with a 2-body sub-resonance.

Starting from the pair production of $pp \rightarrow \Theta\Theta \rightarrow 4g$, the final state contains four jets with a pair of dijet resonances of equal mass, as can be seen in Figure 8. This final state with a pair of dijet resonances has been studied in Refs. [2, 21–23] and searched for at the LHC by both CMS [24, 25] and ATLAS [26, 27]. Using the latest result from ATLAS with 36.7 fb^{-1} data [27], the upper limit on the cross section for production of a color-octet scalar pair is around 0.4 pb for $M_\Theta = 700 \text{ GeV}$, which approximately matches the production cross section predicted in the ReCoM, shown in Figure 6. So, for this region of parameter space, the limit on the color-octet scalar mass is $M_\Theta \gtrsim 700 \text{ GeV}$.

As shown in Figure 6, the Θ pair production is typically dominated by the coloron-

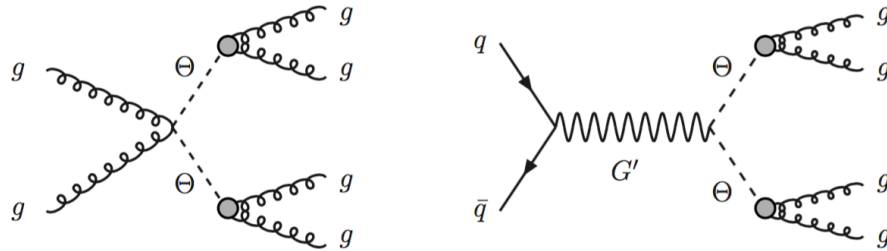


Figure 8: Pair production of the color-octet scalar Θ , through QCD (left-hand diagram; related diagrams with only trilinear vertices are not shown), and coloron decay (right-hand diagram), followed by Θ decays into two gluons at one loop. The branching fraction for $\Theta \rightarrow gg$ is close to 100% when $M_\Theta < M_{\phi_I}$.

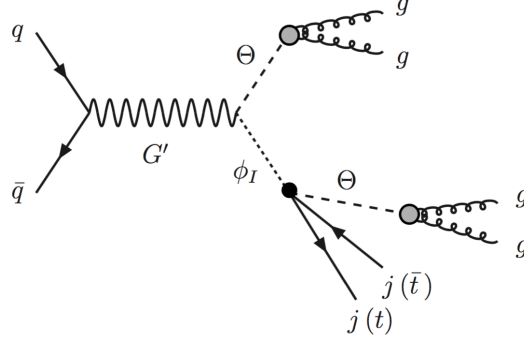


Figure 9: Resonant production of a coloron that decays into an octet scalar Θ and a singlet scalar ϕ_I , which then decays (for $M_\Theta < M_{\phi_I}$) via an off-shell coloron into a Θ plus either two quark jets or $t\bar{t}$.

mediated process when $M_{G'} > 2M_\Theta$. Thus, besides searching for a pair of dijet resonances, one could also search for a resonance in the invariant mass spectrum of all four jets (for a related collider study with b jets at the Tevatron, see [2]).

For a hierarchical mass spectrum with $M_{G'} \gg M_\Theta$, the Θ particle from G' decays could be highly boosted and behave as a jet with 2-prong substructure at the LHC. The latter has an invariant mass given by M_Θ , and we label it by J_Θ . As a rough estimate, the angular separation of the two gluon-jets from Θ decays has a lower bound approximately given by [28]

$$\Delta R_{gg} \simeq \frac{2 M_\Theta}{p_T(\Theta)} \simeq 4 \frac{M_\Theta}{M_{G'}} \quad . \quad (4.1)$$

For instance, one could enlarge the jet-finding-algorithm radius to $R \sim 0.8$ for $M_\Theta = 1$ TeV and $M_{G'} = 5$ TeV and use additional jet-substructure techniques to search for the signal in this case [29].

If the scalars are even more boosted such that the two gluon-jets are within the jet cone used in regular dijet searches, then the $pp \rightarrow G' \rightarrow \Theta\Theta \rightarrow J_\Theta J_\Theta$ process will effectively appear as a dijet resonance. The effective dijet branching fraction of the coloron would then be larger, and the constraint from dijet resonance searches would be stronger (see Figure 7). However, using a typical $\Delta R_{gg} = 0.4$ in Eq. (4.1) would require $M_\Theta/M_{G'} \lesssim O(0.1)$. This in conjunction with the lower limit on M_Θ would push $M_{G'}$ above 7 TeV, where the production cross section becomes too small.

For the singlet scalar, ϕ_I , the main production is together with a Θ scalar via G' decays. The corresponding Feynman diagram for its production and decay is shown in Figure 9. When it is produced at the LHC, the ϕ_I undergoes a 3-body decay into Θ plus a quark pair via an off-shell coloron. When the quark is not the top, the quark pair hadronizes into two jets. After the two Θ 's decay, there are altogether six jets in the final state, with two of them having an invariant mass of M_Θ and four of them an

invariant mass of M_{ϕ_I} : $pp \rightarrow G' \rightarrow \Theta \phi_I \rightarrow \Theta(\Theta q \bar{q}) \rightarrow (gg)((gg)q\bar{q})$. The total invariant mass of all six jets should match the coloron mass $M_{G'}$. To our knowledge, there are no dedicated experimental searches to cover this signature. A less sensitive but related search is looking for microscopic black holes at the 13 TeV LHC via multiple jets [30] with 2.3 fb^{-1} luminosity. Based on a parton-level simulation, we conclude that the upper bound on the cross section for six or more jets does not constrain the ReCoM.

Searches for the signal of multiple resonances in 6-jet final states would suffer from a combinatorial background. For instance, there are $C_6^2 C_4^2 = 90$ dijet pairs if the search is designed to find the two dijet resonances associated with Θ . This combinatorial issue would likely make the reconstructed Θ resonance very broad.

Instead of reconstructing the Θ or ϕ_I resonances, a simple strategy is to use the invariant mass of all six jets to search for the G' resonance. Even then, additional jets from initial state radiation would complicate the reconstruction of the resonance. In addition, the jet energy resolution in the presence of a large number of jets would make the resonance broad.

The situation is dramatically different when $M_{G'} \gg M_{\phi_I} > M_\Theta$. The signal arising from the asymmetric decay of a coloron produced in the s -channel, $pp \rightarrow G' \rightarrow \Theta \phi_I$, is then a “dijet” resonance, with one of the jets (J_Θ) having a 2-prong substructure, and the other jet (of mass M_{ϕ_I} and labelled by $J_{jj\Theta}$) having a 4-prong substructure. In this case, the effective dijet branching fraction is closer to 100% (provided that each multi-prong jet fits inside an $\Delta R = 0.4$ cone), so that the constraint from dijet resonance searches approaches the dotted line in Figure 7.

The case where $M_{G'} > M_{\phi_I} \gg M_\Theta$ would still be phenomenologically different. Note, however, that this case is not consistent with the upper limit $M_{\phi_I} < 2.1 M_\Theta$ derived in the Appendix, which is based on the assumption that the color-preserving vacuum is the global minimum of the scalar potential.

Nevertheless, there are interesting intermediate cases, where $M_{G'}$ is considerably larger than $M_{\phi_I} + M_\Theta$ such that the primary Θ is moderately boosted, while the two quark jets and the Θ arising from the ϕ_I decay have only a small boost. An example of mass spectrum that leads to the above situation is $M_\Theta \approx 1 \text{ TeV}$, $M_{\phi_I} \approx 2 \text{ TeV}$ and $M_{G'} \approx 6 \text{ TeV}$. The signal is a J_Θ , which in this case is a wide jet of $\Delta R_{gg} \approx 0.8$, and four other jets that reconstruct the ϕ_I mass. The reconstruction of the resonances would be improved by techniques that distinguish between gluon jets and quark jets.

A separate class of signatures arises from the $\phi_I \rightarrow t\bar{t}\Theta$ decay (see Figure 9). Even though the branching fraction for this 3-body decay is $1/6$, or smaller when $M_{\phi_I} - M_\Theta$ is near $2m_t$, the more complicated final states associated with top quarks may be used to reduce the backgrounds. For example, one may use the leptonic decay of a W from the $pp \rightarrow G' \rightarrow \phi_I \Theta \rightarrow W^+ W^- b\bar{b} + 4j$ process.

If $M_{G'} \gg M_{\phi_I} > M_\Theta$, then the $\phi_I \rightarrow t\bar{t}\Theta \rightarrow t\bar{t}jj$ system is also boosted, giving rise to an object (we label it by $J_{t\bar{t}\Theta}$) that includes multi-prong jet substructure and sometimes nonisolated leptons and missing energy. The signal is then $pp \rightarrow G' \rightarrow J_\Theta J_{t\bar{t}\Theta}$.

4.2 Light singlet scalar: $M_{G'} > M_\Theta > M_{\phi_I}$

Let us now study the mass ordering where the singlet scalar ϕ_I is lighter than the color-octet scalar Θ . Θ has 2-body decays into two gluons and 3-body decays into $j\bar{j}\phi_I$ with the branching fractions depending on $\tan\theta$ and on the $M_\Theta/M_{G'}$ and $M_{\phi_I}/M_{G'}$ mass ratios, as follows from Eqs. (2.20) and (2.21) (see also Figure 1).

The ϕ_I undergoes 4-body 1-loop decays into two gluons and a quark-antiquark pair, or 2-body 3-loop decays into W^+W^- , γZ or ZZ . The latter are dominant for $M_{\phi_I} < M_0$ where the mass scale M_0 can be derived from Eq. (2.37):

$$M_0 \approx 0.7 \eta_3^{1/4} (\tan\theta M_\Theta M_{G'})^{1/2} . \quad (4.2)$$

As mentioned in Section 2.4, η_3 is a number that accounts for the 3-loop integrals, which are difficult to calculate; we expect η_3 to be of order 1, but values as low as $1/30$ or so would not be very surprising.

4.2.1 $\phi_I \rightarrow ggq\bar{q}$

Let us first focus on the $M_{\phi_I} > M_0$ case, implying that ϕ_I decays predominantly into $ggq\bar{q}$. An interesting process (see right diagram of Figure 10) is s -channel coloron production followed by the asymmetric coloron decay into $\Theta\phi_I$, and leading to a ten jet final state: $pp \rightarrow G' \rightarrow \Theta\phi_I \rightarrow (\phi_I q\bar{q})\phi_I \rightarrow ((ggq\bar{q})q\bar{q})(ggq\bar{q}) \rightarrow 10j$. Each parenthesis here denotes the presence of a resonance.

Depending on the masses of the three ReCoM bosons, some of these jets may be merged. In particular, when $M_{G'}$ and M_Θ have the same order of magnitude while the

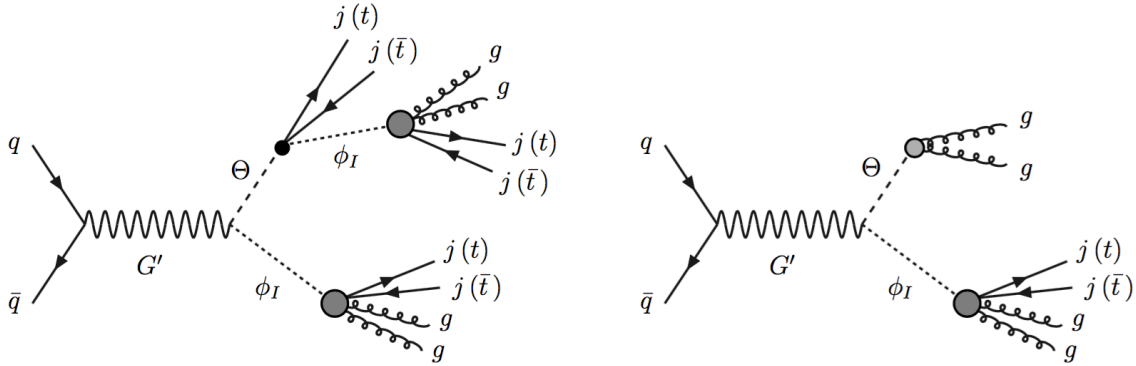


Figure 10: Asymmetric $pp \rightarrow G' \rightarrow \phi_I\Theta$ processes for $M_\Theta > M_{\phi_I}$, when the ϕ_I scalar decays into two gluons plus two quarks, which occurs at one-loop (see Figure 3). Left diagram: scalar pair production is followed by a 3-body decay of the color-octet Θ into ϕ_I plus a quark-antiquark pair, which forms two jets, or less often a $t\bar{t}$ pair. Right diagram: Θ decays into two gluons, at one loop.

scalar masses satisfy $M_\Theta \gg M_{\phi_I}$ and $M_{G'} - M_\Theta \gg M_{\phi_I}$, the final state includes four jets with two of them having each a 4-prong substructure and an invariant mass given by M_{ϕ_I} . We use the notation J_{ϕ_I} for such a jet formed by the merger of two gluons and two quark jets arising from a ϕ_I decay. The above cascade decay of the coloron is then $G' \rightarrow \Theta \phi_I \rightarrow J_{\phi_I} J_{\phi_I} j j$. If $M_{G'} - M_\Theta$ is near M_{ϕ_I} (a more tuned situation) and $M_\Theta \gg M_{\phi_I}$, then the signal consists of seven jets, with only one of them being an J_{ϕ_I} . For $M_{G'} \gg M_\Theta > M_{\phi_I}$, the whole $q\bar{q}\phi_I \rightarrow q\bar{q}(ggq'\bar{q}')$ system (labelled by $J_{jj\phi_I}$) is boosted, and is approximately back-to-back against a J_{ϕ_I} (we will see though below that the branching fraction for $\Theta \rightarrow q\bar{q}\phi_I$ is small in this case).

There is also a $pp \rightarrow G' \rightarrow \Theta \phi_I \rightarrow (gg)(ggq\bar{q}) \rightarrow 6j$ process, where two gluon jets reconstruct the Θ mass, and the other four jets reconstruct the ϕ_I mass. So far, no search in the six jet final state has been performed by imposing a separate mass constraint for two different resonances. Even though the intermediate states are different than in the process shown in Figure 9 and discussed in Section 4.1, the final state is identical. Nevertheless, the range of parameters here is larger than in the case discussed in Section 4.1, leading to novel boosted topologies. For $M_{G'} > M_\Theta \gg M_{\phi_I}$ the resonant signal has three jets, with one of them being an J_{ϕ_I} , and the other two jets forming a resonance at M_Θ . Requiring the total invariant mass of three jets match the G' mass should provide a sensitive way to test these signatures. Using a simple estimate where the system of the four partons is boosted in the shape of a tetrahedron, we find that $\phi_I \rightarrow ggq\bar{q}$ fits inside a cone of

$$\Delta R_{ggq\bar{q}} \simeq \frac{2\sqrt{2} M_{\phi_I}}{p_T(\phi_I)} \simeq \frac{4\sqrt{2} M_{\phi_I}}{M_{G'} (1 - M_\Theta^2/M_{G'}^2)} \quad . \quad (4.3)$$

Thus, one could identify the J_{ϕ_I} jet using a normal jet-finding radius $R \sim 0.8$ for $M_{\phi_I} \approx 0.8$ TeV, $M_\Theta \approx 1$ TeV and $M_{G'} \approx 6$ TeV.

The quark-antiquark pair arising from either $\Theta \rightarrow q\bar{q}\phi_I$ or $\phi_I \rightarrow ggq\bar{q}$ decays may be a $t\bar{t}$ pair, albeit the branching fraction is only 1/6 (or smaller if there is kinematic suppression), as opposed to 5/6 for light SM quarks. In the case of the $G' \rightarrow \Theta \phi_I \rightarrow (\phi_I q\bar{q})\phi_I \rightarrow ((ggq\bar{q})q\bar{q})(ggq\bar{q})$ cascade decay, the probability of having one of the quark-antiquark pairs to be $t\bar{t}$ can be as large as 34.7%, and even the case where there are two $t\bar{t}$ pairs is potentially relevant, having a probability of 6.9% (without taking into account the G' and Θ branching fractions). Thus, if there are no large mass hierarchies, the signatures include $t\bar{t} + 8j$ and $4t + 6j$. If $M_{\phi_I} \ll M_{G'}$, then the final states include J_{ϕ_I} jets with 4-prong substructure, or boosted $t\bar{t}gg$ systems (we label them by $J_{t\bar{t}gg}$) with an invariant mass equal again to M_{ϕ_I} . The latter have various interesting signatures; for example, when only one of the W bosons produced by the top quarks decays leptonically, the boosted $t\bar{t}gg \rightarrow \ell b\bar{b} + 4j + \cancel{E}_T$ system will include a non-isolated lepton aligned with the missing energy. Even more complicated objects occur when $M_{G'} \gg M_\Theta > M_{\phi_I}$. A boosted $\Theta \rightarrow t\bar{t} + 4j$ (or less often $\Theta \rightarrow 4t + jj$) system is then produced approximately back-to-back with a $J_{t\bar{t}gg}$.

The main LHC signatures arising from the asymmetric $pp \rightarrow G' \rightarrow \Theta \phi_I$ process are summarized in Figure 11 (also including channels discussed in Section 4.1). Note that

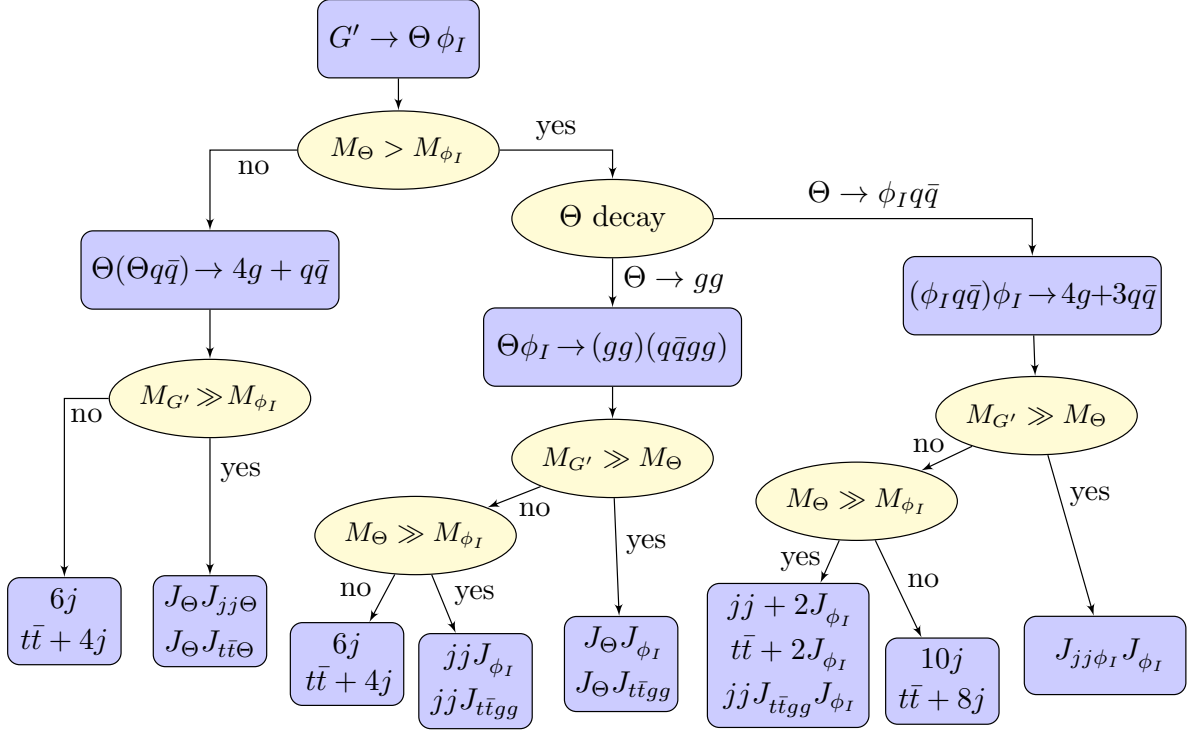


Figure 11: Signatures of the ReCoM from the asymmetric $pp \rightarrow G' \rightarrow \Theta \phi_I$ production, and the corresponding mass relations. For $M_{\phi_I} < M_{\Theta}$, only the 1-loop $\phi_I \rightarrow ggq\bar{q}$ decays are included here. The jet labelled by J_{Θ} has a 2-prong substructure, while $J_{jj\phi_I}$ has a 6-prong substructure; both have an invariant mass given by M_{Θ} . The jets labelled by J_{ϕ_I} and $J_{jj\Theta}$ have a 4-prong substructure and an M_{ϕ_I} invariant mass. The boosted objects labelled by $J_{t\bar{t}gg}$ and $J_{t\bar{t}\Theta}$ have more complicated substructure and an M_{ϕ_I} invariant mass. For $M_{\phi_I} \lesssim O(1 \text{ TeV})$ and $M_{\phi_I} < M_{\Theta}$, ϕ_I is so long-lived that J_{ϕ_I} and $J_{t\bar{t}gg}$ may have a displaced origin.

some final states that require parameter tuning, or have smaller branching fractions, are not shown there.

For $2M_{\Theta} > M_{G'} > M_{\Theta} + M_{\phi_I}$, the asymmetric channel $G' \rightarrow \Theta \phi_I$ is open and has a large branching fraction, while the symmetric $G' \rightarrow \Theta \Theta$ channel is kinematically closed (even then, the QCD production of a pair of Θ scalars leads to many of the additional final states discussed in what follows).

For $M_{G'} > 2M_{\Theta} > M_{\Theta} + M_{\phi_I}$, both the asymmetric and the symmetric channels are open. Note that there is interference between the $pp \rightarrow G' \rightarrow \Theta \Theta$ and QCD Θ pair production. The symmetric coloron decays lead to a variety of signatures in addition to those from Figure 11. Pair production of the color-octet scalar followed by each Θ decaying into $jj\phi_I$ leads to a twelve jet final state: $pp \rightarrow \Theta \Theta \rightarrow \phi_I \phi_I + 4j \rightarrow 12j$ (see

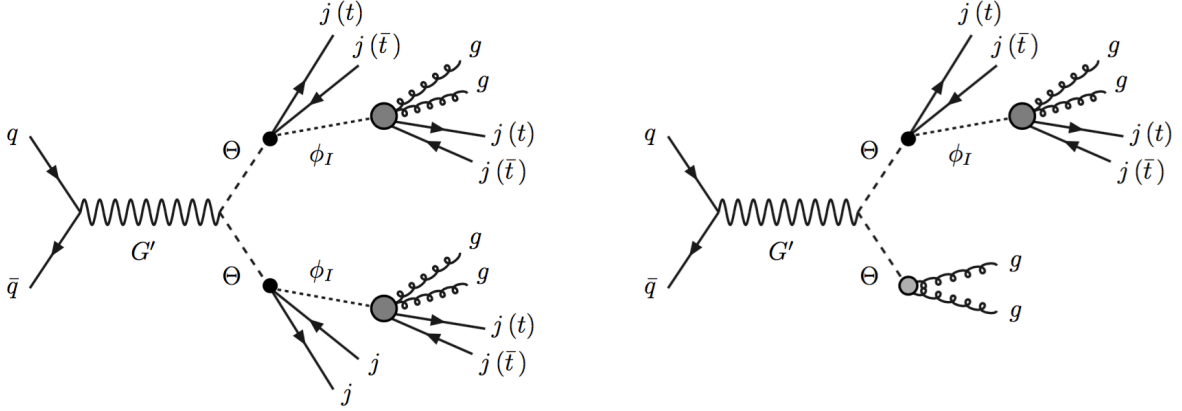


Figure 12: Resonant production of a coloron that decays into a pair of color-octet scalars, for $M_\Theta > M_{\phi_I}$ when the singlet scalar decays into two gluons plus two quarks. Left diagram: both Θ scalars undergo a cascade decay through an off-shell coloron. Right diagram: one Θ has a cascade decay, the other one decays at 1-loop into two gluons.

the left diagram of Figure 12) if the main decay of ϕ_I is $\phi_I \rightarrow g g q \bar{q}$ at one loop. The searches for microscopic black holes via multi-jet final states [30] may become sensitive to this ReCoM signal after the LHC accumulates enough luminosity. Specific to ReCoM, searching for a resonance in the invariant mass spectrum of all twelve jets can substantially improve the search sensitivity.

For the parameter region with $M_\Theta \gg M_{\phi_I}$, the ϕ_I from Θ decays is likely to be boosted. Thus, the signature is $pp \rightarrow \Theta\Theta \rightarrow J_{\phi_I} J_{\phi_I} + 4j$. A possible search strategy is to require two jets to have a 4-prong substructure and approximately the same mass. In addition, one may try to reconstruct the Θ mass from the $C_4^2 = 6$ pairs of 3-jet resonances, similar to the searches for gluinos undergoing R parity violating decays [31–33].

If the $\Theta \rightarrow \phi_I q \bar{q}$ and $\Theta \rightarrow gg$ decays have comparable branching fractions, then the process $pp \rightarrow \Theta\Theta \rightarrow (\phi_I q \bar{q})(gg) \rightarrow 8j$ (see the right diagram of Figure 12) has a large rate. For $M_\Theta \gg M_{\phi_I}$, the final state becomes $J_{\phi_I} + 4j$. This has the same combinatorial factor of 6 for reconstructing the intermediate Θ resonance.

A substantial 3-body branching fraction for Θ requires that the mass ratio of $M_\Theta/M_{G'}$ is not too small (see Figure 1). As a result, the 3-body decaying Θ is less likely to be boosted. To be more precise, for $M_{\phi_I} \ll M_\Theta \ll M_{G'}$ Eqs. (2.20) and (2.21) imply a ratio of branching fractions

$$\begin{aligned} \frac{B(\Theta \rightarrow \phi_I j j, \phi_I t \bar{t})}{B(\Theta \rightarrow gg)} &\simeq \frac{4\pi \tan^2 \theta}{405 \alpha_s (\pi^2/9 - 1)^2 (1 + r_A)^2} \left(\frac{M_\Theta}{M_{G'}} \right)^2 \\ &\approx 0.1 \left(\frac{\tan \theta}{0.4} \right)^2 \left(\frac{M_\Theta}{1 \text{ TeV}} \right)^2 \left(\frac{5 \text{ TeV}}{M_{G'}} \right)^2, \end{aligned} \quad (4.4)$$

where the 3-body branching fraction is summed over all six flavors and $r_A \approx 0.53$. The

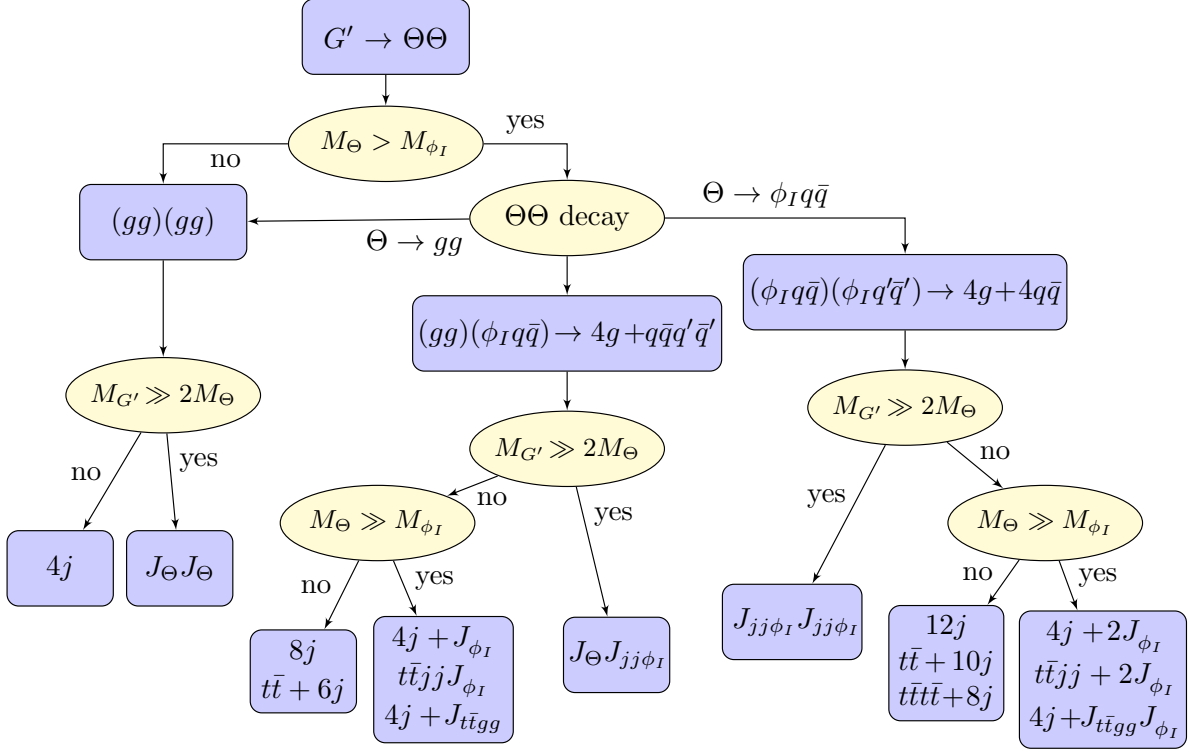


Figure 13: Same as Figure 11, except that the final states shown here arise from the $pp \rightarrow G' \rightarrow \Theta\Theta$ process.

three jets produced in the $\Theta \rightarrow \phi_I q \bar{q} \rightarrow J_{\phi_I} j j$ decay fit inside an $\Delta R = 0.8$ cone provided $0.8 \gtrsim \sqrt{3} M_\Theta / p_T(\Theta) \simeq 2\sqrt{3} M_\Theta / M_{G'}$, so that Eq. (4.4) implies an upper limit on the 3-body branching fraction, $B(\Theta \rightarrow \phi_I j j, \phi_I t \bar{t}) \lesssim 12\%$ for $\tan \theta = 0.4$. Note that at this point in parameter space, which is almost optimal for a boosted Θ undergoing a 3-body decay, the branching fractions of G' into scalars are only $B(G' \rightarrow \Theta\Theta) = 16\%$ and $B(G' \rightarrow \Theta\phi_I) = 32\%$.

In the processes discussed above, each of the quark-antiquark pairs from the Θ and ϕ_I decays may be a $t\bar{t}$ pair, with a branching fraction of $1/6$ (for $M_\Theta - M_{\phi_I} \gg 2m_t$ and $M_{\phi_I} \gg 2m_t$). Thus, the process where both Θ 's undergo cascade decays (left diagram in Figure 12) includes a single $t\bar{t}$ pair with a probability of 38.6%, and exactly two $t\bar{t}$ pairs with a probability of 11.6%.

Pair production of Θ followed by both Θ 's decaying to gg has been discussed in Section 4.1. The main signatures of ReCoM arising from the $G' \rightarrow \Theta\Theta$ decays are summarized in Figure 13. Certain processes with smaller branching fractions, such as $\Theta\Theta \rightarrow (\phi_I t \bar{t})(\phi_I t \bar{t})$, are not included there.

The $\phi_I \rightarrow g g q \bar{q}$ decays are either prompt or displaced depending on the values of the

four parameters (M_{ϕ_I} , M_Θ , $M_{G'}$, $\tan\theta$) that enter the 4-body width given in Eqs. (2.28) and (2.26). The proper decay length of ϕ_I is approximately proportional to $M_{G'}^6 M_\Theta^4 / M_{\phi_I}^{11}$, assuming that there is no fine tuning of the M_Θ / M_{ϕ_I} ratio. A ϕ_I produced in coloron decays has a boost $\gamma_{\phi_I} = E_{\phi_I} / M_{\phi_I}$, where E_{ϕ_I} is the energy of a ϕ_I in the lab frame. The decay length of ϕ_I in the lab frame is then

$$\begin{aligned} \lambda_4(\phi_I) &\approx \frac{663 (4\pi)^4 \tan^2\theta}{\alpha_s^5 (1 + \tan^2\theta)^4} \frac{M_{G'}^6 M_\Theta^4}{M_{\phi_I}^{12}} E_{\phi_I} \\ &= O(0.03 \text{ cm}) \left(\frac{\tan\theta}{0.3} \right)^2 \left(\frac{700 \text{ GeV}}{M_{\phi_I}} \right)^{12} \left(\frac{M_{G'}}{3 \text{ TeV}} \right)^7 \left(\frac{M_\Theta}{1 \text{ TeV}} \right)^4 \frac{E_{\phi_I}}{M_{G'}/6}. \end{aligned} \quad (4.5)$$

In the last line we assumed $\tan^2\theta \ll 1$. Note that the coloron is expected to be produced with small momentum, so the process $pp \rightarrow G' \rightarrow \Theta\Theta \rightarrow (\phi_I q \bar{q})(\phi_I q \bar{q})$ leads to a ϕ_I energy $E_{\phi_I} \sim O(M_{G'}/6)$ for a typical event, while the process $pp \rightarrow G' \rightarrow \Theta\phi_I \rightarrow (\phi_I q \bar{q})\phi_I$ leads to a slightly larger E_{ϕ_I} .

The existing searches for displaced dijet resonances set an upper limit on the production cross section of a pair of displaced jets in the range of 1–10 fb for decay lengths larger than $O(1)$ mm and smaller than a meter or so [34] at the 13 TeV LHC. As this topology occurs in the ReCoM for $M_{G'} \gtrsim 5$ TeV, for example from the $G' \rightarrow \Theta\phi_I \rightarrow jj J_\phi J_\phi$ process with displaced J_ϕ , the production cross section shown in Figure 5 is not yet constrained.

4.2.2 $\phi_I \rightarrow W^+W^-, \gamma Z, ZZ$

When ϕ_I is lighter than both Θ and the scale M_0 introduced in Eq. (4.2), its leading decays are into two electroweak gauge bosons (with the exception of two photons) and occur at three loops, as in the right-hand diagram in Figure 4. To find the LHC signatures, one can repeat the previous discussion with the 4-body decay $\phi_I \rightarrow ggq\bar{q}$ replaced by the 2-body ones. The branching fractions of $\phi_I \rightarrow W^+W^-, \gamma Z, ZZ$ are 65%, 19%, 16%, respectively, or smaller if the $\phi_I \rightarrow ggq\bar{q}$ width is not negligible.

The signatures of asymmetric coloron decays are $G' \rightarrow \Theta\phi_I \rightarrow (\phi_I q \bar{q} / t \bar{t})\phi_I \rightarrow 2(\gamma Z / ZZ / W^+W^-) + jj / t \bar{t}$ when Θ has 3-body decays, and $\Theta\phi_I \rightarrow (\gamma Z / ZZ / W^+W^-) + jj$ in the case of $\Theta \rightarrow gg$. Pair production of the color-octet scalars, through QCD and s -channel G' , leads to $\Theta\Theta \rightarrow (\phi_I q \bar{q})(\phi_I q \bar{q}) \rightarrow 2(\gamma Z / ZZ / W^+W^-) + 4j$ and the same with one or two $q\bar{q}$ pairs replaced by $t\bar{t}$ pairs, as well as $\Theta\Theta \rightarrow (\phi_I q \bar{q})(gg) \rightarrow (\gamma Z / ZZ / W^+W^-) + 4j$, as shown for example in Figure 14. Note that the boson pairs tend to be boosted given that $M_{\phi_I} \lesssim 1$ TeV in this case, while the coloron has a mass of several TeV. We will use the notation J_{WW} , $J_{\gamma Z}$ and J_{ZZ} for a boosted di-boson system of invariant mass equal to M_{ϕ_I} , independent of how the W or Z bosons decay.

For hadronic decays of ZZ and W^+W^- , ϕ_I could still behave as a 4-prong jet with two internal Z or W -jets. For the final states with a photon or leptonic decays of Z and W bosons, the collider signatures contain $\gamma \ell^+ \ell^- + \text{jets}$, $\gamma + \cancel{E}_T + \text{jets}$, $\ell^\pm + \cancel{E}_T + \text{jets}$,

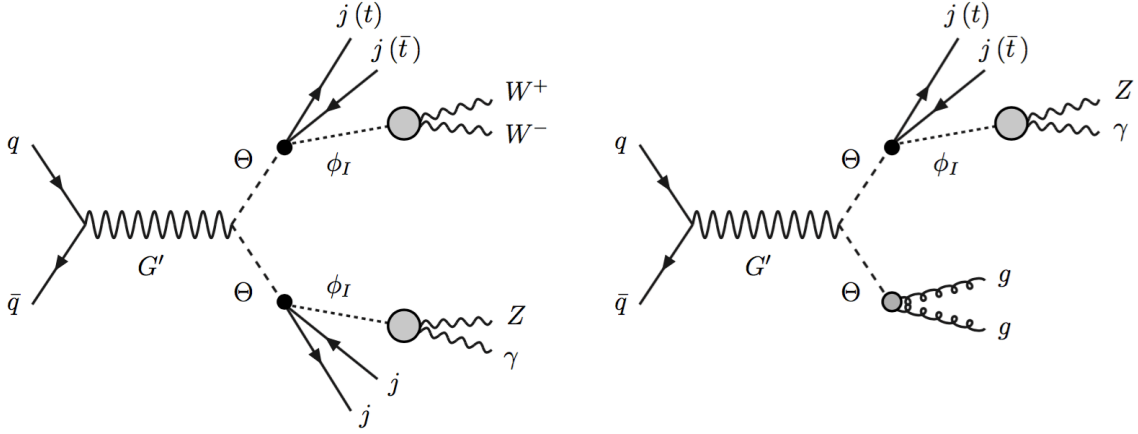


Figure 14: Representative LHC processes from symmetric coloron decays, for $M_\Theta > M_{\phi_I}$ when ϕ_I decays into pairs of electroweak bosons at three loops (represented by the largest gray disc). The γZ and W^+W^- systems are likely to be boosted and to originate from displaced vertices.

$\ell^+\ell^- + \cancel{E}_T + \text{jets}$, or more leptons when there are up to four weak bosons from two ϕ_I decays.

The 2-body partial widths of ϕ_I , given in Eq. (2.36), imply that the lab-frame decay length of ϕ_I in this case is

$$\begin{aligned} \lambda_2(\phi_I) &\approx \frac{4(4\pi)^6 c_W^4 s_W^4}{25 \eta_3^2 \alpha^2 \alpha_s^5 \tan^2 \theta (1 + \tan^2 \theta)^4 (3c_W^4 + s_W^4)} \frac{M_{G'}^2}{M_{\phi_I}^4} E_{\phi_I} \\ &= O(0.03 \text{ cm}) \left(\frac{\tan \theta}{0.3} \right)^2 \left(\frac{700 \text{ GeV}}{\sqrt{\eta_3} M_{\phi_I}} \right)^4 \left(\frac{M_{G'}}{3 \text{ TeV}} \right)^3 \frac{E_{\phi_I}}{M_{G'}/6}. \end{aligned} \quad (4.6)$$

Note the milder dependence on M_{ϕ_I} compared to Eq. (4.5), as well as the dependence on the numerical coefficient η_3 . In most cases the $\phi_I \rightarrow W^+W^-, \gamma Z, ZZ$ decays are associated with displaced vertices. For η_3 of order one, the displacement varies between the millimeter scale (for $\phi_I \gtrsim 500 \text{ GeV}$) and the meter scale (for $\phi_I \approx 100 \text{ GeV}$), while for η_3 of order 0.1 the displacement grows by two orders of magnitude. Thus, we expect WW , γZ and ZZ resonances which are both boosted and displaced. So far there have been no dedicated collider searches for boosted systems with displaced vertices.

The $\phi_I \rightarrow \gamma Z$ decay may in principle be constrained by existing searches with non-pointing photons without special requirement of jet multiplicity [35]. For the lifetime of the long-lived particle in the range of 250 ps to about 100 ns, the upper limit on the signal production cross section at the 8 TeV LHC ranges from 1 fb to 100 fb. By comparing to the 13 TeV LHC cross section for the production of a Θ pair shown in Figure 6, and multiplying by the branching fractions for one of the Θ 's to decay into $\phi q \bar{q}$ and also for $\phi_I \rightarrow \gamma Z$, we derive a lower limit on M_Θ of roughly 0.7 TeV when the coloron is not

too heavy [so that the 3-body ϕ branching fraction is not too suppressed, see Eq. (4.4)]. The signal sensitivity can be improved by also requiring the presence of high p_T jets. Therefore, for a ϕ_I mass below about 700 GeV, searches with a displaced $J_{\gamma Z}$ and prompt high- p_T jets could lead to a clean discovery.

When $M_{\phi_I} < M_Z$, which is a natural region of parameter space given that ϕ_I is a pseudo-Nambu Goldstone boson, the main decays of ϕ_I are 3-loop 3-body processes, which include a photon and proceed via an off-shell Z boson: $\phi_I \rightarrow \gamma jj, \gamma \nu \bar{\nu}, \gamma \ell^+ \ell^-$. The decay length is then longer than the detector, so ϕ_I behaves as a missing particle in collider experiments. The collider signatures of coloron decays then include missing transverse energy plus prompt jets or top quark pairs when there are 3-body Θ decays, or plus a dijet resonance when one of the Θ decays into two gluons.

5 Discussion and conclusions

The ReCoM is a UV-complete gauge extension of QCD. The sector that spontaneously breaks the $SU(3)_1 \times SU(3)_2$ gauge symmetry includes a color-octet scalar (Θ) and two singlet scalars (ϕ_I and ϕ_R). It is natural that Θ and ϕ_I are lighter than the coloron, as they are pNGB's associated with an $SO(18) \rightarrow SO(17)$ global symmetry breaking. In addition, ϕ_I is the pNGB associated with the breaking of a global $U(1)_\Sigma$ symmetry.

All the SM quarks are triplets under one (the first, by convention) of the $SU(3)$ gauge groups, so the coloron has flavor-universal couplings. The ReCoM belongs to a small but remarkable class of gauge extensions of the SM that does not require anomalous, *i.e.*, fermions beyond the SM quarks and leptons that cancel the gauge anomalies.¹

As there are no significant constraints on the coloron from flavor-changing processes² or electroweak observables, the only relevant limits on the coloron mass ($M_{G'}$) and coupling ($\tan \theta$) are set by searches at the LHC. Dijet resonance searches set the limits in the $(\tan \theta, M_{G'})$ plane shown in Figure 7. The $t\bar{t}$ resonance searches are weaker because the coloron branching fraction into $t\bar{t}$ is smaller than the jj one by a factor of 5.

For $\tan \theta \lesssim 0.45$, the dominant coloron decays are into a pair of scalars. The $G' \rightarrow \Theta \phi_I$ decay has typically the largest branching fraction (unless $M_{\phi_I} > M_\Theta$ and $M_{G'}$ is near $M_{\phi_I} + M_\Theta$), but the $G' \rightarrow \Theta\Theta$ branching fraction is also substantial (see Figure 2). The subsequent decays of Θ and ϕ_I lead to a variety of final states, depending on four parameters: $M_{G'}$, M_Θ , M_{ϕ_I} and $\tan \theta$. When $M_{\phi_I} > M_\Theta$, the color octet Θ decays into a pair of gluons, and ϕ_I decays into $jj\Theta$, so that the final state includes up to six jets, with some of them merged depending on how light the scalars are compared to the coloron.

When $M_{\phi_I} < M_\Theta$, the main decays of Θ are into $q\bar{q}\phi_I$ (where q is a SM quark jet),

¹Another gauge extension of QCD without anomalous is $SU(3)_1 \times SU(3)_2 \times SU(3)_3$ with each generation of SM quarks charged under a different $SU(3)$ (see also [36] for a possible solution to the strong \mathcal{CP} problem based on this product of gauge groups).

²Flavor constraints are stringent [37] in models where the SM quarks transform under different $SU(3)_1 \times SU(3)_2$ representations.

$t\bar{t}\phi_I$ or gg , while the decays of ϕ_I have highly suppressed widths. The latter include 3-loop 2-body decays (into W^+W^- , γZ or ZZ), as well as 1-loop 4-body decays (into $ggq\bar{q}$ or $gg\bar{t}t$). The ratio of these widths is estimated in Eq. (2.37), where the parameter η_3 introduced in Eq. (2.35) accounts for the uncertainty arising from the 3-loop integrals (computing these is beyond the scope of this paper). We expect that η_3^2 lies between $O(1)$ and $O(10^{-3})$, but even this large uncertainty has a relatively small impact on the possible final states due to the dependence on high powers of the masses (*e.g.*, the ratio of widths is proportional to $M_{\phi_I}^8$). For M_{ϕ_I} larger than the mass scale M_0 [see Eq. (4.2)], which is of the order of 1 TeV, the main decay is $\phi_I \rightarrow q\bar{q}gg$. Although this may be a prompt decay for larger values of M_{ϕ_I} , it may also lead to displaced vertices [see Eq. (4.5)]. Final states with top quarks have smaller branching fractions (in some cases only by a factor of 5/4 or 5/3, if there are four or three quark-antiquark pairs) but are still promising. The final states with multiple jets or top quarks are shown in Table 1. For $M_{\phi_I} \ll M_{G'}$, the $ggq\bar{q}$ system is boosted and forms a jet with 4-prong substructure (labelled by J_{ϕ_I}), while the boosted $ggt\bar{t}$ system is even more complicated.

For M_{ϕ_I} lighter than the mass scale M_0 , the main decay is into a pair of electroweak bosons (W^+W^- , γZ , ZZ), and the decay length of ϕ_I varies between a fraction of millimeter to longer than 1 cm [see Eq. (4.6)]. For $M_{\phi_I} < M_Z$, the main decay is a 3-loop 3-body decay into a photon and an off-shell Z boson; in that case the decay is likely to be outside the detector, so ϕ_I would appear as missing transverse energy. The channels with electroweak bosons that have large branching fractions, and which do not rely on fine tuning of masses, are shown in Table 2.

So far there have been dedicated searches for very few of the final states listed in Tables 1 and 2. Even though some of these final states can be lumped in certain multi-jet or multi-lepton searches, it is important for the ATLAS, CMS and LHCb collaborations to perform dedicated searches for each of these final states. The sensitivity of a dedicated search far exceeds that of a generic search, especially when the signature involves nested resonances, multi-prong jet substructure, non-isolated leptons or photons, or displaced vertices. Furthermore, depending on the parameter values and the improvements in experimental techniques, any of these signatures may become a discovery mode.

Some of these final states are also encountered in other models. For example, the dominant signals in the ReCoM for a range of masses are $J_{\phi_I}jj$ or $J_{\phi_I} + 4j$, with a narrow J_{ϕ_I} . These would appear as a $3j$ or $5j$ resonance, respectively, which so far have not been searched for. The former is also predicted in models where a vector-like quark is produced at 1-loop in the s -channel, from a gluon-quark initial state, and decays via a dimension-6 operator into three SM quarks.

Even dijet resonance searches, if augmented by substructure techniques, may reveal unusual final states, such as $J_{jj\Theta}J_\Theta$, in which one jet has a 4-prong substructure and the other jet has a 2-prong substructure and a smaller mass. Other final states are more peculiar, such as those with a large number of electroweak bosons (*e.g.*, $\gamma ZW^+W^- + 4j$ or $W^+W^-W^+W^-t\bar{t}jj$), or those involving a displaced γZ resonance. Clearly, there are many new opportunities for new physics searches at the LHC.

partonic process from G' decay	final state	mass relation
$\Theta\phi_I \rightarrow \Theta(\Theta q\bar{q}) \rightarrow (gg)((gg)q\bar{q})$	$6j$ $J_\Theta J_{jj\Theta}$	$M_{G'} > M_{\phi_I} > M_\Theta$ $M_{G'} \gg M_{\phi_I} > M_\Theta$
$\Theta\phi_I \rightarrow (\phi_I q\bar{q})\phi_I \rightarrow ((ggq\bar{q})q\bar{q})(ggq\bar{q})$	$10j$ $J_{\phi_I} + 6j$ $J_{\phi_I} J_{\phi_I} jj$	$M_{G'} > M_\Theta > M_{\phi_I}$ $M_{G'} - M_\Theta \gg M_{\phi_I}$ $M_{G'} > M_\Theta \gg M_{\phi_I}$
$\Theta\phi_I \rightarrow (gg)(ggq\bar{q})$	$6j$ $J_{\phi_I} jj$ $J_\Theta J_{\phi_I}$	$M_{G'} > M_\Theta > M_{\phi_I}$ $M_{G'} - M_\Theta \gg M_{\phi_I}$ $M_{G'} \gg M_\Theta > M_{\phi_I}$
$\Theta\Theta \rightarrow (\phi_I q\bar{q})(\phi_I q\bar{q}) \rightarrow ((ggq\bar{q})q\bar{q})((ggq\bar{q})q\bar{q})$	$12j$ $J_{\phi_I} J_{\phi_I} + 4j$	$M_\Theta > M_{\phi_I}$ $M_\Theta \gg M_{\phi_I}$
$\Theta\Theta \rightarrow (\phi_I q\bar{q})(gg) \rightarrow ((ggq\bar{q})q\bar{q})(gg)$	$8j$ $J_{\phi_I} + 4j$	$M_\Theta > M_{\phi_I}$ $M_\Theta \gg M_{\phi_I}$
$\Theta\Theta \rightarrow (gg)(gg)$	$4j$ $J_\Theta J_\Theta$	$M_{G'} \gg 2M_\Theta$
$\Theta\phi_I \rightarrow (\phi_I q\bar{q})\phi_I \rightarrow (ggt\bar{t})(ggq\bar{q})q\bar{q}$	$t\bar{t} + 8j$ $J_{ggt\bar{t}} J_{\phi_I} jj$	$M_{G'} > M_\Theta > M_{\phi_I}$ $M_{G'} > M_\Theta \gg M_{\phi_I}$
$\Theta\Theta \rightarrow (\phi_I t\bar{t}/q\bar{q})(\phi_I q\bar{q}) \rightarrow (ggq\bar{q}t\bar{t})((ggq\bar{q})q\bar{q})$	$t\bar{t} + 10j$ $J_{ggt\bar{t}} J_{\phi_I} + 4j$ $t\bar{t} J_{\phi_I} J_{\phi_I} jj$	$M_\Theta > M_{\phi_I}$ $M_\Theta \gg M_{\phi_I}$
$\Theta\Theta \rightarrow (\phi_I t\bar{t}/q\bar{q})(\phi_I t\bar{t}/q\bar{q}) \rightarrow (ggq\bar{q}t\bar{t})(ggq\bar{q}t\bar{t})$	$t\bar{t}t\bar{t} + 8j$ $t\bar{t} J_{ggt\bar{t}} J_{\phi_I} jj$ $J_{ggt\bar{t}} J_{ggt\bar{t}} + 4j$ $t\bar{t}t\bar{t} J_{\phi_I} J_{\phi_I}$	$M_\Theta > M_{\phi_I}$ $M_\Theta \gg M_{\phi_I}$
$\Theta\Theta \rightarrow (\phi_I t\bar{t}/q\bar{q})(gg) \rightarrow (ggq\bar{q}t\bar{t})(gg)$	$t\bar{t} + 6j$ $J_{ggt\bar{t}} + 4j$ $t\bar{t} J_{\phi_I} jj$	$M_\Theta > M_{\phi_I}$ $M_\Theta \gg M_{\phi_I}$

Table 1: Main LHC processes predicted in the ReCoM when $M_{\phi_I} > M_\Theta$, or when $M_{\phi_I} < M_\Theta$ with ϕ_I decaying to $ggq\bar{q}$. Each parenthesis represents a resonance. J_{ϕ_I} is a jet with 4-prong substructure arising from a boosted $\phi_I \rightarrow ggq\bar{q}$, and $J_{ggt\bar{t}}$ is a boosted $\phi_I \rightarrow ggt\bar{t}$. Depending on the parameters from Eq. (4.5), J_{ϕ_I} and $J_{ggt\bar{t}}$ may have a displaced vertex for $M_{\phi_I} \lesssim 1$ TeV. J_Θ is a jet with 2-prong substructure due to a boosted $\Theta \rightarrow gg$. $J_{jj\Theta}$ is a jet with 4-prong substructure due to a boosted ϕ_I . Additional channels are less likely to occur (*e.g.*, $\Theta\Theta \rightarrow J_{jj\phi_I} J_\Theta$, or $\Theta\phi_I \rightarrow 4t + 6j$).

partonic process from G' decay	final state	mass relation
$\Theta\phi_I \rightarrow (\phi_I q\bar{q})\phi_I \rightarrow ((WW)q\bar{q})(WW)$	$W^+W^-W^+W^-jj$ $W^+W^-J_{WW}jj$ $J_{WW}J_{WW}jj$	$M_{G'} > M_\Theta > M_{\phi_I}$ $M_{G'} - M_\Theta \gg M_{\phi_I}$ $M_{G'} > M_\Theta \gg M_{\phi_I}$
$\Theta\phi_I \rightarrow (\phi_I q\bar{q})\phi_I \rightarrow (WW)(\gamma Z)q\bar{q}$	γZW^+W^-jj $\gamma ZJ_{WW}jj$ $W^+W^-J_{\gamma Z}jj$ $J_{\gamma Z}J_{WW}jj$	$M_\Theta > M_{\phi_I}$ $M_{G'} - M_\Theta \gg M_{\phi_I}$ $M_{G'} - M_\Theta \gg M_{\phi_I}$ $M_\Theta \gg M_{\phi_I}$
$\Theta\phi_I \rightarrow (gg)(WW)$	W^+W^-jj $J_{WW}jj$ $J_{WW}J_\Theta$	$M_\Theta > M_{\phi_I}$ $M_{G'} - M_\Theta \gg M_{\phi_I}$ $M_{G'} \gg M_\Theta > M_{\phi_I}$
$\Theta\phi_I \rightarrow (gg)(\gamma Z)$	γZjj $J_{\gamma Z}jj$ $J_{\gamma Z}J_\Theta$	$M_\Theta > M_{\phi_I}$ $M_{G'} - M_\Theta \gg M_{\phi_I}$ $M_{G'} \gg M_\Theta > M_{\phi_I}$
$\Theta\Theta \rightarrow (\phi_I q\bar{q})(\phi_I q\bar{q}) \rightarrow ((WW)q\bar{q})((WW)q\bar{q})$	$4W + 4j$ $J_{WW}J_{WW} + 4j$	$M_\Theta > M_{\phi_I}$ $M_\Theta \gg M_{\phi_I}$
$\Theta\Theta \rightarrow (\phi_I q\bar{q})(\phi_I q\bar{q}) \rightarrow ((\gamma Z)q\bar{q})((WW)q\bar{q})$	$\gamma ZW^+W^- + 4j$ $J_{\gamma Z}J_{WW} + 4j$	$M_\Theta > M_{\phi_I}$ $M_\Theta \gg M_{\phi_I}$
$\Theta\Theta \rightarrow (\phi_I q\bar{q})(gg) \rightarrow ((WW)q\bar{q})(gg)$	$W^+W^- + 4j$ $J_{WW} + 4j$	$M_\Theta > M_{\phi_I}$ $M_\Theta \gg M_{\phi_I}$
$\Theta\Theta \rightarrow (\phi_I q\bar{q})(gg) \rightarrow ((\gamma Z)q\bar{q})(gg)$	$\gamma Z + 4j$ $J_{\gamma Z} + 4j$	$M_\Theta > M_{\phi_I}$ $M_\Theta \gg M_{\phi_I}$
$\Theta\Theta \rightarrow (\phi_I t\bar{t})(\phi_I q\bar{q}) \rightarrow ((WW)t\bar{t})((WW)q\bar{q})$	$4W + t\bar{t}jj$ $J_{WW}J_{WW}t\bar{t}jj$	$M_\Theta > M_{\phi_I}$ $M_\Theta \gg M_{\phi_I}$
$\Theta\Theta \rightarrow (\phi_I t\bar{t})(\phi_I q\bar{q}) \rightarrow (\gamma Z)(WW)t\bar{t}q\bar{q}$	$\gamma ZW^+W^-t\bar{t}jj$ $J_{\gamma Z}J_{WW}t\bar{t}jj$	$M_\Theta > M_{\phi_I}$ $M_\Theta \gg M_{\phi_I}$

Table 2: LHC processes predicted in the ReCoM when $M_{\phi_I} < M_\Theta$ and $\phi_I \rightarrow WW$ or γZ . J_{WW} and $J_{\gamma Z}$ represent a W^+W^- or γZ system produced in the decay of a boosted ϕ_I . These originate from a displaced vertex for $M_{\phi_I} \lesssim 1$ TeV, and may appear as \cancel{E}_T for $M_{\phi_I} \lesssim 100$ GeV. Additional channels (*e.g.*, those involving two $t\bar{t}$ pairs or $\phi_I \rightarrow ZZ$) have smaller branching fractions. The mass relations displayed here are necessary but not sufficient (*e.g.*, $\gamma ZJ_{WW}jj$ also requires that M_Θ is not much larger than M_{ϕ_I}).

Acknowledgments: We thank Sida Lu, Nhan Tran and Qianfei Xiang for useful discussions and comments. The work of YB is supported by the U. S. Department of Energy under the contract DE-SC0017647. The work of BD has been supported by Fermi Research Alliance, LLC under Contract No. DE-AC02-07CH11359 with the U.S. Department of Energy, Office of Science, Office of High Energy Physics.

Appendix: Ratios of scalar masses

We now derive the allowed range for the scalar mass ratio M_{ϕ_I}/M_Θ . As mentioned in Section 2, in the limit $\mu_\Sigma \rightarrow 0$, the potential has a global $U(1)_\Sigma$ symmetry, which is broken by the Σ VEV. The corresponding Nambu-Goldstone is ϕ_I , so that $M_{\phi_I}/M_\Theta \rightarrow 0$ for $\mu_\Sigma \rightarrow 0$.

The upper limit of M_{ϕ_I}/M_Θ is more complicated to derive. Let us first use Eq. (2.5) to write

$$\frac{M_{\phi_I}}{M_\Theta} = \sqrt{3} \left(2 + \frac{\sqrt{2} \kappa f_\Sigma}{\sqrt{3} \mu_\Sigma} \right)^{-1/2}. \quad (\text{A.1})$$

The necessary and sufficient condition for the potential $V(\Sigma)$ [see Eq. (2.1)] to be bounded from below, derived in [11], is

$$\kappa > \max \{ -\lambda, -3\lambda \} \quad . \quad (\text{A.2})$$

Imposing this condition, and using the expression of the VEV value f_Σ in terms of the potential parameters given in Eq. (2.3), the scalar mass ratio becomes

$$\frac{M_{\phi_I}}{M_\Theta} = \sqrt{3\lambda + \kappa} \left(2\lambda + \kappa + \frac{\kappa}{3} \sqrt{4(3\lambda + \kappa) \frac{m_\Sigma^2}{\mu_\Sigma^2} + 1} \right)^{-1/2}. \quad (\text{A.3})$$

The condition (A.2) implies $2\lambda + \kappa > 0$, so that the maximum value of M_{ϕ_I}/M_Θ occurs at $\kappa < 0$ and $m_\Sigma^2 > 0$. Furthermore, m_Σ^2/μ_Σ^2 must be maximized to reach the maximum for M_{ϕ_I}/M_Θ . The vacuum that preserves $SU(3)_c$ is the global minimum for $\kappa < 0$ (which implies $\lambda > 0$) and $m_\Sigma^2 > 0$ provided [11]

$$(3\lambda + \kappa) \frac{m_\Sigma^2}{\mu_\Sigma^2} \leq \mathcal{G}(\kappa/\lambda) \quad , \quad (\text{A.4})$$

where the function $\mathcal{G}(x)$ is defined on the interval $-1 < x < 0$ by

$$\mathcal{G}(x) = (3 + x) \left(\frac{(4 + 2x)^{3/2}}{\sqrt{1 + x}} - 2(4 + x) \right)^{-1}. \quad (\text{A.5})$$

Note that if the inequality (A.4) is not satisfied, then the gauge symmetry breaking pattern in the global minimum is $SU(3)_1 \times SU(3)_2 \rightarrow SU(2) \times SU(2) \times U(1)$, so color is broken. Nevertheless, an $SU(3)_c$ -symmetric local minimum still exists [11] for slightly larger values of m_Σ^2/μ_Σ^2 . We will not consider here the possibility that the viable vacuum is not the global minimum.

The constraint (A.4) implies the following upper limit:

$$\frac{M_{\phi_I}}{M_\Theta} \leq R_{\max}(\kappa/\lambda) \quad , \quad (\text{A.6})$$

where the function introduced here is

$$R_{\max}(x) = \frac{\sqrt{3+x}}{\left(2+x+(x/3)\sqrt{4\mathcal{G}(x)+1}\right)^{1/2}} \quad . \quad (\text{A.7})$$

For any values of the quartic couplings that satisfy $-1 < \kappa/\lambda < 0$ we find that the upper limit for the mass ratio is above $\sqrt{3}$. The maximum value $(M_{\phi_I}/M_\Theta)_{\max} = 3/\sqrt{2}$ is reached at $\kappa \rightarrow 0$. Hence, the ReCoM predicts

$$M_{\phi_I} \lesssim 2.1 M_\Theta \quad . \quad (\text{A.8})$$

Let us now find the maximum values of M_{ϕ_I}/M_Θ in other regions of parameter space. For $\kappa \geq 0$ and $m_\Sigma^2 > 0$ the only vacuum is $SU(3)_c$ symmetric. From Eq. (A.3), the maximum of M_{ϕ_I}/M_Θ is obtained when $m_\Sigma^2 \rightarrow 0$, so that

$$\frac{M_{\phi_I}}{M_\Theta} \leq \sqrt{\frac{3\lambda + \kappa}{2\lambda + 4\kappa/3}} \quad . \quad (\text{A.9})$$

The range of M_{ϕ_I}/M_Θ consistent with a viable global minimum is shown as a function of κ/λ in Figure 15. The solid blue line there is the upper limit for $\kappa < 0$, given in (A.6), while the dashed blue line represents the upper limit (A.9) for $\kappa > 0$.

For $m_\Sigma^2 < 0$, the $SU(3)_c$ symmetric vacuum is the global minimum provided [11]

$$(3\lambda + \kappa) \frac{m_\Sigma^2}{\mu_\Sigma^2} > -\frac{2}{9} \quad . \quad (\text{A.10})$$

If this is not satisfied, the $SU(3)_1 \times SU(3)_2$ gauge symmetry is unbroken. If $\kappa < 0$, then the maximum is at $m_\Sigma^2 \rightarrow 0$ and given by (A.9). If $\kappa > 0$ and $m_\Sigma^2 < 0$, then M_{ϕ_I}/M_Θ reaches its maximum when the above inequality is saturated:

$$\frac{M_{\phi_I}}{M_\Theta} \leq \sqrt{\frac{3\lambda + \kappa}{2\lambda + 10\kappa/9}} \quad . \quad (\text{A.11})$$

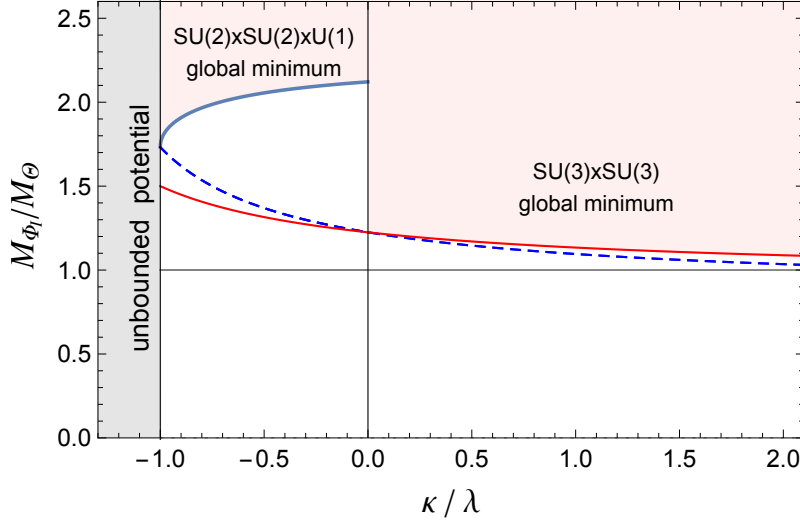


Figure 15: Allowed range (unshaded region) for the scalar mass ratio M_{ϕ_I}/M_{Θ} as a function of the quartic coupling ratio κ/λ . In the pink shaded region the global minimum does not preserve color (for $\kappa/\lambda < 0$) or the extended gauge symmetry is unbroken (for $\kappa/\lambda > 0$). In the gray shaded region the potential is not bounded from below. The upper limit on M_{ϕ_I}/M_{Θ} is given by the solid blue line for $m_{\Sigma}^2 > 0$ and $\kappa < 0$; the solid red line for $m_{\Sigma}^2 > 0$ and $\kappa < 0$; the dashed blue line for $\kappa m_{\Sigma}^2 > 0$.

The above upper limit is shown as the solid red lines in Figure 15. The conclusion is that even though it is natural to have $M_{\phi_I} < M_{\Theta}$, the opposite mass relation, $M_{\phi_I} > M_{\Theta}$, also occurs for sizable regions of parameter space.

For the other singlet scalar, ϕ_R , the squared mass given in Eq. (2.5) may be rewritten using the expression of the Σ VEV, f_{Σ} , from (2.3):

$$M_{\phi_R}^2 = \frac{f_{\Sigma}}{\sqrt{6}} \sqrt{4(3\lambda + \kappa)m_{\Sigma}^2 + \mu_{\Sigma}^2} \quad . \quad (\text{A.12})$$

For $m_{\Sigma}^2 < 0$, the condition (A.10) implies

$$\frac{1}{3} < \frac{M_{\phi_R}}{M_{\phi_I}} < \frac{1}{\sqrt{3}} \quad . \quad (\text{A.13})$$

For $m_{\Sigma}^2 > 0$, the condition (A.2) for the potential to be bounded from below implies a lower limit on M_{ϕ_R}/M_{ϕ_I} :

$$\frac{M_{\phi_R}}{M_{\phi_I}} > \frac{1}{\sqrt{3}} \quad . \quad (\text{A.14})$$

Note that ϕ_R is much heavier than other scalars when $\lambda \gg |\kappa|$ and $m_{\Sigma}^2 \gg \mu_{\Sigma}^2$.

References

- [1] T. P. Cheng and L. F. Li, *Gauge theory of elementary particle physics*. Oxford Science Publications, 1984.
- [2] Y. Bai and B. A. Dobrescu, *Heavy octets and Tevatron signals with three or four b jets*, *JHEP* **07** (2011) 100, [[arXiv:1012.5814](#)].
- [3] B. A. Dobrescu and A. D. Peterson, *W' signatures with odd Higgs particles*, *JHEP* **08** (2014) 078, [[arXiv:1312.1999](#)].
- [4] C. T. Hill, *Topcolor: Top quark condensation in a gauge extension of the standard model*, *Phys. Lett.* **B266** (1991) 419–424.
- [5] C. T. Hill and S. J. Parke, *Top production: Sensitivity to new physics*, *Phys. Rev.* **D49** (1994) 4454–4462, [[hep-ph/9312324](#)].
- [6] R. S. Chivukula, A. G. Cohen, and E. H. Simmons, *New strong interactions at the Tevatron?*, *Phys. Lett.* **B380** (1996) 92–98, [[hep-ph/9603311](#)].
- [7] E. H. Simmons, *Coloron phenomenology*, *Phys. Rev.* **D55** (1997) 1678–1683, [[hep-ph/9608269](#)].
- [8] L. J. Hall and A. E. Nelson, *Heavy Gluons and Monojets*, *Phys. Lett.* **153B** (1985) 430.
- [9] P. H. Frampton and S. L. Glashow, *Chiral Color: An Alternative to the Standard Model*, *Phys. Lett.* **B190** (1987) 157–161.
- [10] J. Bagger, C. Schmidt, and S. King, *Axigluon Production in Hadronic Collisions*, *Phys. Rev.* **D37** (1988) 1188.
- [11] Y. Bai and B. A. Dobrescu, *Minimal $SU(3) \times SU(3)$ symmetry breaking patterns*, [arXiv:1710.01456](#).
- [12] R. S. Chivukula, A. Farzinnia, J. Ren, and E. H. Simmons, *Constraints on the Scalar Sector of the Renormalizable Coloron Model*, *Phys. Rev.* **D88** (2013), no. 7 075020, [[arXiv:1307.1064](#)]. [Erratum: *Phys. Rev.* **D89**, no. 5, 059905 (2014)].
- [13] R. S. Chivukula, E. H. Simmons, A. Farzinnia, and J. Ren, *LHC Constraints on a Higgs boson Partner from an Extended Color Sector*, *Phys. Rev.* **D90** (2014), no. 1 015013, [[arXiv:1404.6590](#)].
- [14] E. Nardi, *Naturally large Yukawa hierarchies*, *Phys. Rev.* **D84** (2011) 036008, [[arXiv:1105.1770](#)].

- [15] J. R. Espinosa, C. S. Fong, and E. Nardi, *Yukawa hierarchies from spontaneous breaking of the $SU(3)_L \times SU(3)_R$ flavour symmetry?*, *JHEP* **02** (2013) 137, [[arXiv:1211.6428](#)].
- [16] R. S. Chivukula, A. Farzinia, J. Ren, and E. H. Simmons, *Hadron Collider Production of Massive Color-Octet Vector Bosons at Next-to-Leading Order*, *Phys. Rev.* **D87** (2013), no. 9 094011, [[arXiv:1303.1120](#)].
- [17] A. D. Martin, W. J. Stirling, R. S. Thorne, and G. Watt, *Parton distributions for the LHC*, *Eur. Phys. J.* **C63** (2009) 189–285, [[arXiv:0901.0002](#)].
- [18] **CMS** Collaboration, V. Khachatryan et al., *Searches for dijet resonances in pp collisions at $\sqrt{s} = 13$ TeV using data collected in 2016*, *report* [PAS-EXO-16-056](#).
- [19] **ATLAS** Collaboration, M. Aaboud et al., *Search for new phenomena in dijet events using 37 fb^{-1} of pp collision data collected at $\sqrt{s} = 13$ TeV*, [arXiv:1703.09127](#).
- [20] **CMS** Collaboration, A. M. Sirunyan et al., *Search for $t\bar{t}$ resonances in highly boosted lepton+jets and fully hadronic final states in proton-proton collisions at $\sqrt{s} = 13$ TeV*, *JHEP* **07** (2017) 001, [[arXiv:1704.03366](#)].
- [21] B. A. Dobrescu, K. Kong, and R. Mahbubani, *Massive color-octet bosons and pairs of resonances at hadron colliders*, *Phys. Lett.* **B670** (2008) 119–123, [[arXiv:0709.2378](#)].
- [22] R. S. Chivukula, M. Golden, and E. H. Simmons, *Multi-jet physics at hadron colliders*, *Nucl. Phys.* **B363** (1991) 83–96.
- [23] C. Kilic, T. Okui, and R. Sundrum, *Colored Resonances at the Tevatron: Phenomenology and Discovery Potential in Multijets*, *JHEP* **07** (2008) 038, [[arXiv:0802.2568](#)].
- [24] **CMS** Collaboration, S. Chatrchyan et al., *Search for pair-produced dijet resonances in four-jet final states in pp collisions at $\sqrt{s}=7$ TeV*, *Phys. Rev. Lett.* **110** (2013), no. 14 141802, [[arXiv:1302.0531](#)].
- [25] **CMS** Collaboration, V. Khachatryan et al., *Search for pair-produced resonances decaying to jet pairs in proton-proton collisions at $\sqrt{s} = 8$ TeV*, *Phys. Lett.* **B747** (2015) 98–119, [[arXiv:1412.7706](#)].
- [26] **ATLAS** Collaboration, M. Aaboud et al., *A search for pair produced resonances in four jets final states in proton-proton collisions at $\sqrt{s}=13$ TeV*, *report* [CONF-2016-084](#).
- [27] **ATLAS** Collaboration, M. Aaboud et al., *A search for pair-produced resonances in four-jet final states at $\sqrt{s} = 13$ TeV*, *report* [CONF-2017-025](#).

- [28] J. M. Butterworth, A. R. Davison, M. Rubin, and G. P. Salam, *Jet substructure as a new Higgs search channel at the LHC*, *Phys. Rev. Lett.* **100** (2008) 242001, [[arXiv:0802.2470](#)].
- [29] Y. Bai and J. Shelton, *Composite Octet Searches with Jet Substructure*, *JHEP* **07** (2012) 067, [[arXiv:1107.3563](#)].
- [30] **CMS** Collaboration, V. Khachatryan et al., *Search for Black Holes with Early Run 2 Data*, Tech. Rep. CMS-PAS-EXO-15-007, CERN, Geneva, 2015.
- [31] **CMS** Collaboration, S. Chatrchyan et al., *Searches for light- and heavy-flavour three-jet resonances in pp collisions at $\sqrt{s} = 8$ TeV*, *Phys. Lett.* **B730** (2014) 193–214, [[arXiv:1311.1799](#)].
- [32] **ATLAS** Collaboration, G. Aad et al., *Search for massive supersymmetric particles decaying to many jets using the ATLAS detector in pp collisions at $\sqrt{s} = 8$ TeV*, *Phys. Rev.* **D91** (2015), no. 11 112016, [[arXiv:1502.05686](#)]. [Erratum: *Phys. Rev.* **D93**, no. 3, 039901 (2016)].
- [33] **ATLAS** Collaboration, M. Aaboud et al., *Search for massive supersymmetric particles in multi-jet final states produced in pp collisions at $\sqrt{s} = 13$ TeV*, [report CONF-2016-057](#).
- [34] **CMS** Collaboration, V. Khachatryan et al., *Inclusive search for new particles decaying to displaced jets at $\sqrt{s} = 13$ TeV*, [report PAS-EXO-16-003](#).
- [35] **ATLAS** Collaboration, G. Aad et al., *Search for nonpointing and delayed photons in the diphoton and missing transverse momentum final state in 8 TeV pp collisions at the LHC using the ATLAS detector*, *Phys. Rev.* **D90** (2014), no. 11 112005, [[arXiv:1409.5542](#)].
- [36] P. Agrawal and K. Howe, *A Flavorful Factoring of the Strong CP Problem*, [arXiv:1712.05803](#).
- [37] R. S. Chivukula, E. H. Simmons, and C. P. Yuan, *Axiguons cannot explain the observed top quark forward-backward asymmetry*, *Phys. Rev.* **D82** (2010) 094009, [[arXiv:1007.0260](#)].